Behavioral/Systems/Cognitive

Active and Passive Antennal Movements during Visually Guided Steering in Flying *Drosophila*

Akira Mamiya, Andrew D. Straw, Egill Tómasson, and Michael H. Dickinson
Divisions of Biology and Engineering and Applied Science, California Institute of Technology, Pasadena, California 91125

Insects use feedback from a variety of sensory modalities, including mechanoreceptors on their antennae, to stabilize the direction and speed of flight. Like all arthropod appendages, antennae not only supply sensory information but may also be actively positioned by control muscles. However, how flying insects move their antennae during active turns and how such movements might influence steering responses are currently unknown. Here we examined the antennal movements of flying *Drosophila* during visually induced turns in a tethered flight arena. In response to both rotational and translational patterns of visual motion, *Drosophila* actively moved their antennae in a direction opposite to that of the visual motion. We also observed two types of passive antennal movements: small tonic deflections of the antenna and rapid oscillations at wing beat frequency. These passive movements are likely the result of wing-induced airflow and increased in magnitude when the angular distance between the wing and the antenna decreased. In response to rotational visual motion, increases in passive antennal movements appear to trigger a reflex that reduces the stroke amplitude of the contralateral wing, thereby enhancing the visually induced turn. Although the active antennal movements significantly increased antennal oscillation by bringing the arista closer to the wings, it did not significantly affect the turning response in our head-fixed, tethered flies. These results are consistent with the hypothesis that flying *Drosophila* use mechanosensory feedback to detect changes in the wing induced airflow during visually induced turns and that this feedback plays a role in regulating the magnitude of steering responses.

Introduction

During locomotion, all animals must integrate input from sensory receptors that are moving with respect to the environment. These movements may allow efficient sampling of sensory information (Schroeder et al., 2010) but could also make it difficult to distinguish sensory signals generated by self-motion from those generated by changes in the environment (Cullen, 2004). Studying how animals process information from moving sensors is critical for understanding the mechanisms underlying sensorimotor transformation during active behavior in a natural setting. The antennae of insects are an interesting example of this problem because they not only move with the animal as it explores but can also be actively positioned relative to the head (Honegger et al., 1990; Bauer and Gewecke, 1991; Kloppenburg, 1995; Ehmer and Gronenberg, 1997; Kloppenburg et al., 1997; Dürr et al., 2001; Baba and Comer, 2008). In flying insects, active movements of the antennae may prevent saturation of the antennal mechanoreceptors used to control airspeed (Heran, 1959; Burkhardt and Gewecke, 1965; Gewecke, 1970). Recently, it has also been proposed that flying *Drosophila* may actively move the antennae to activate mechanoreceptors that initiate saccadic turns toward odor plumes (Duistermars et al., 2009; Duistermars and Frye, 2010). However, how flies actually move their antennae during active turns and what functional role, if any, such movements play remain unknown. As an initial step in addressing these questions, we used a machine vision system to track the movements of antennae in *Drosophila* during visually induced turns.

The antennae of *Drosophila* are composed of three segments: the scape, the pedicel, and the funiculus. The joint between the scape and the pedicel (SP joint) is actuated by two muscles (Hartenstein, 2006), whereas the joint between the pedicel and the funiculus (PF joint) moves passively (Schneider, 1964). By restricting the movements of these two joints, we analyzed how the antennae move during visually induced turns and investigated the roles that active and passive joint movements might play. We identified a stereotyped optomotor reflex of the antennae in which flies actively rotate their SP joint in the direction opposite to that of large field visual motion. We also observed two types of passive movements of the PF joint: a slow, tonic deflection and a fast oscillation at wing beat frequency (WBF). These passive movements increased in amplitude when the distance between the antenna and the ipsilateral wing stroke envelope narrowed and are likely caused by wing-induced airflow. Such passive movements of the PF joint might serve a number of different functions, including enhancing the steering reaction to rotational visual motion by activating Johnston's organ (JO) neurons that reduce the contralateral stroke amplitude. Although active antennal movements significantly increase the antennal oscillations by bringing the antenna closer to the ipsilateral wing, they did not significantly affect the turning response in our head-

Received Jan. 28, 2011; revised March 10, 2011; accepted March 17, 2011.

Author contributions: A.M., A.D.S., and M.H.D. designed research; A.M. performed research; A.D.S. and E.T. contributed unpublished reagents/analytic tools; A.M. analyzed data; A.M. and M.H.D. wrote the paper.

This work was supported by National Science Foundation Frontiers in Integrative Biological Research Award 0623527 (M.H.D.). We thank Martin Peek for technical assistance and Gaby Maimon for helpful discussion and comments.

Correspondence should be addressed to Akira Mamiya, Division of Biology and Engineering and Applied Science, California Institute of Technology, Mail Code 138-78, 1200 East California Boulevard, Pasadena, CA 91125. E-mail: mamiya@caltech.edu.

DOI:10.1523/JNEUROSCI.0498-11.2011

 0270-6474/11/316900-15$15.00/0

fixed, tethered flies. Our results are consistent with the hypothesis that flying *Drosophila* use mechanosensory feedback to detect changes in the wing-induced air currents during visually induced turns and that this feedback modulates steering responses.

Materials and Methods

Preparation of flies. We used 3- to 4-d-old female *Drosophila melanogaster* from our laboratory culture originated from 200 wild-caught females. Because the overlap of legs and antennae in video images interfere with our ability to track antennal angles (see below), we anesthetized the flies by cooling them using a Peltier stage held at ~4°C and cutoff their prothoracic legs at the coxa-trochanter joint. The legs were excised at least 4 h before the experiments to provide sufficient recovery time. Preliminary data showed that this procedure does not alter the optomotor responses of either the wings or antennae. For flies used to assess the role of the JO, we glued one antenna at the PF joint using UV-cured glue (Duro) (Budick et al., 2007) immediately after removing their prothoracic legs. Several previous studies have used this gluing procedure successfully to interfere with JO function (Budick et al., 2007; Duistermars et al., 2009; Robie et al., 2010). For assessing the role of the wing-induced air currents on passive movements of the PF joint, we cut off the distal two-thirds of one wing, starting our incision at the distal edge of the costal cell on the leading edge.

Thirty minutes before each experiment, we anesthetized the flies again and glued a tungsten rod (0.1 mm diameter) to the anterior notum using the UV-cured glue. During the experiments, the flies were held in a hovering posture with a pitch angle of ~60° from horizontal (Fig. 1*A*). For accurate measurements of the antenna angles, we immobilized the head by gluing it to the tungsten rod at a nose-down pitch of ~30°. In some experiments, we interfered with the motion of the antenna by gluing the SP joint (which the antennal muscles actuate) with the UV-cured glue while the flies were attached to their tether and flying. Gluing the joint while the flies were flying was necessary because the flies actively raise their antennae when they fly, and it was difficult to fix the SP joint at a position that approximated its normal flight position while they were anesthetized.

Flight arena and visual stimuli. Details of the visual display used in these experiments have been described previously (Reiser and Dickinson, 2008). We inserted the flies into a center of an arena consisting of 32 rows × 88 columns of light-emitting diodes (LEDs) covering 330° in azimuth and 94° in elevation around the fly (Fig. 1*A*). A 30° gap in the rear, approximating the blind spot of the fly, was used for inserting the tethered flies into the arena. At the middle of the arena, each LED subtends a visual angle of 3.75° on the fly's retina, which is smaller than the interommatidial distance of *Drosophila* (Heisenberg and Wolf, 1984). The luminance of the fully lit arena was 72 cd/m^2, and the maximum relative (Michelson) contrast of the display was ~93% (Reiser and Dickinson, 2008).

To induce turning responses in flies, we presented four different types of large-field visual motion by moving a vertical square-wave pattern with a fundamental spatial frequency of 60° (30° of fully lit LEDs, 30° of dark LEDs) around the fly. We moved the pattern either rotationally [clockwise (CW) or counterclockwise (CCW)] or translationally [rightward translation (RT) with a focus of expansion and contraction located 90° to the left and right of the fly, respectively, or leftward translation (LT) with a focus of expansion and contraction reversed from the RT pattern]. The temporal frequency of the motion stimuli was set at 6.12 Hz, which is in a range known to evoke the strongest turning responses for these two classes of stimuli (Duistermars et al., 2007).

Each trial started with a display of a stationary square wave pattern (0.84 s duration), followed by visual motion of the pattern (2.94 s duration), and then another stationary pattern (1.17 s duration). Between trials, flies were presented with a dark 30° wide, 94° tall stripe on a bright background under standard closed-loop conditions for 5 s, in which the animals themselves control the angular velocity of the stripe via feedback from the wing beat analyzer. Flies in closed-loop conditions tend to keep a vertical stripe centered in front of them by balancing their left and right wing stroke amplitudes (Reichardt and Wenking, 1969; Götz, 1987),

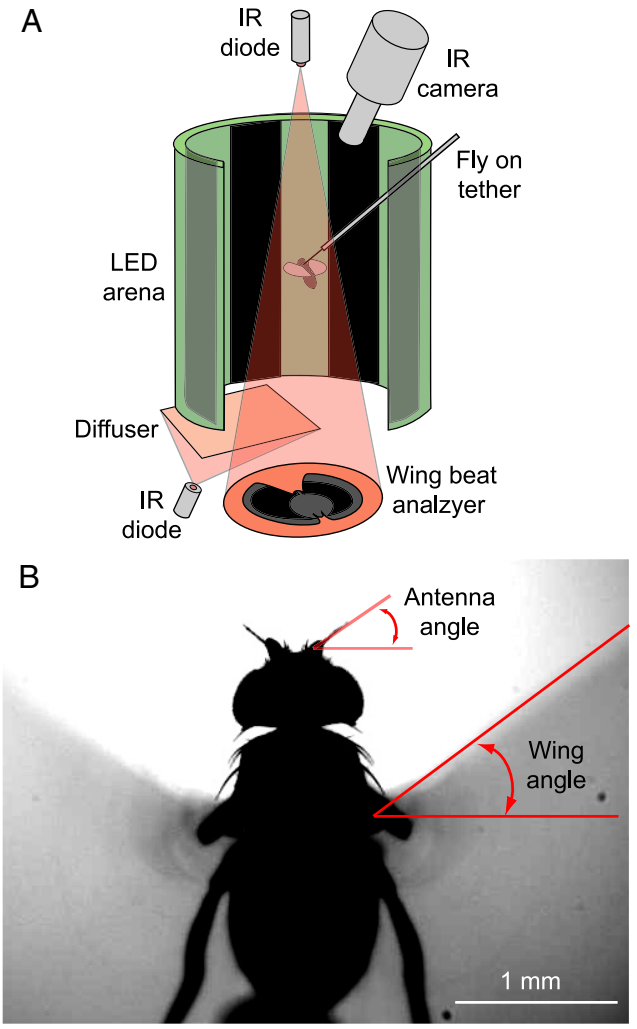

Figure 1. Schematic of the experimental setup. ***A***, Tethered flies were placed in the center of a cylindrical LED array at a pitch angle of ~60° from horizontal. For optical recordings of wing stroke amplitude, we illuminated the fly from above using IR diode and measured the shadows of the wings cast on the wing beat analyzer below the fly. For tracking antennae angles and calibrating the wing angles, we illuminated a light diffuser below the fly with an IR diode and recorded images of the antennae and wings with a light diffuser as a background using an IR-sensitive camera positioned above. In the schematic, the 30° empty sector of the LED display behind the fly is shown larger for illustration purposes. ***B***, An example of an image used for calculating the angles of the antennae and the wings. In the image, the aristae and the wings appear as dark shadows against a brightly lit background. Antenna and wing angles were calculated within the image plane and were defined as the angle between the arista, or the front edge of the wing envelope, and the horizontal axis of the image, respectively. For the right antennae and wings, CCW rotation was defined as positive angles. For the left antennae and wings, CW rotation was defined as positive angles.

providing unbiased initial conditions before each motion trial. The stationary pattern was presented before and after the motion stimulus to more cleanly separate the responses to visual motion from the response elicited by a transition from closed to open loop. Each block of trials consisted of four types of visual motion (CW, CCW, RT, LT) presented once each in random order and each fly was presented with 15–21 blocks of trials. Trials in which flies stopped flying were removed from the analysis. For each pattern of visual motion, only flies with >10 complete trials were included in the analysis.

Presentation of a constant airflow. To present a constant airflow from the front, we used a small open-throat wind tunnel consisting of an electric fan that drove air through a 9-mm-diameter plastic tube. We removed one LED panel from the arena directly in front of the fly and placed the plastic tube through that opening. The open end of the tube

was positioned 20 mm in front of the fly's head. We set the airflow to 0.42 m/s, which was calibrated using a hot wire anemometer placed at the location where the fly's head would be during an experiment. This value was chosen because it is within the range of airspeeds observed when the flies fly freely within an indoor flight arena (Budick and Dickinson, 2006).

Measurement of the antenna and the wing angles. To track the movements of antennae, we used a Basler A602f camera with a fixed-focus lens (Infinistix 90, 94 mm working distance, 1.0× magnification) and recorded images of antennae at 500 frames/s using Motmot, an open source camera software written in Python (Straw and Dickinson, 2009). The camera was pitched down 25° from the horizontal plane to capture the image of the funiculus and the arista from the top of the head (Fig. 1*A*,*B*). We illuminated a light diffuser located below the fly with a high-intensity infrared (IR) diode (880 nm; Golden Dragon; Osram) so that the aristae were imaged as dark silhouettes on a bright background (Fig. 1*B*). Only a small region of interest (22 × 22 pixels, 8.65 μm/pixel) around each arista was used for analysis. We calculated the angle of the arista relative to the horizontal axis of the image (Fig. 1*B*) in real time using a computer algorithm written as a plug-in to FView, a graphical user interface included in Motmot. This algorithm detected pixels with intensities lower than the user-specified value and calculated the eigenvectors of the covariance matrix of this intensity-thresholded image. Each arista appeared as a straight line in the intensity-thresholded images, and an eigenvector with the largest eigenvalue corresponded well with its orientation in the image. Because the arista and the funiculus are known to rotate together as a single solid body (Göpfert and Robert, 2001, 2002), measuring the angle of the arista allowed us to track the angle of the funiculus in the image plane. We report the orientation of the arista as "antenna angle" (Fig. 1*B*). We defined CW and CCW rotation as positive angle for the left and the right antenna, respectively, so that rostral rotations correspond to positive changes in the antenna angle for both sides.

We visually inspected all videos and tracking data offline to check for any gross tracking errors. In ~34% of the trials (2605 of 7641 trials), the mesothoracic legs occasionally overlapped with aristae in the image causing error in the calculation of the antenna angle. These events were usually very brief in time (<8 ms), and visual inspection of the tracking traces showed sudden large changes in the antenna angle (>15°) from one data point to another. When these errors occurred, we removed the antenna angle data within an 8 ms window surrounding the error and linearly interpolated the missing points using the data immediately before and after the removed section. In ~3% of the trials (232 of 7641 trials), overlap of the legs and aristae lasted longer than 8 ms, and these trials were removed from the analysis.

We monitored the fly's wing stroke amplitudes using an optical wing beat analyzer (JFI Electronics Laboratory, University of Chicago) in which we illuminate the wing with an IR diode and record the shadow cast by the wing over infrared sensors (Götz, 1987; Lehmann and Dickinson, 1997) (Fig. 1*A*). We digitized the outputs from the wing beat analyzer together with the command sent to the visual display at 512.8 Hz using CamTrig USB Device included in Motmot. This device synchronized the timestamps for the acquired data with the timestamps of the camera images, allowing us to estimate the wing stroke amplitude and the visual stimuli at the time the antenna image was acquired through linear interpolation of the acquired data.

The wing beat analyzer generates a voltage value for each wing stroke that is proportional to the angular position of the wing at the ventral reversal point, where the wing undergoes the downstroke-to-upstroke transition. To convert these relative measurements of the wing stroke into absolute angles, we calculated the angle of the wing at the ventral reversal point from images of the wing stroke envelope (Fig. 1*B*) acquired at 100 frames/s using a plug-in for Motmot (Maimon et al., 2010) and simultaneously recorded the outputs from the wing beat analyzer using the CamTrig USB Device mentioned above. We constructed calibration curves for each fly, by plotting wing angle calculated from the images against the corresponding output from the wing beat analyzer for two blocks of trials (Hesselberg and Lehmann, 2009) and fit the data with a third-degree polynomial curves using MATLAB (MathWorks). The outputs from the wing beat analyzer recorded during the antennal tracking experiments were converted to wing angles using these calibration curves. To be consistent with our presentation of wing and antenna data, we do not report wing stroke measurements as "stroke amplitude" as is typical of previous studies using calibrated wing beat analyzers (Lehmann and Dickinson, 1997). Stroke amplitude values are obtained by adding 90° to wing angle, assuming that the dorsal reversal occurs at a point parallel to the body axis near the dorsal midline. As with the antennal angles, we defined CW and CCW rotation of the wing envelopes as positive for the left and the right wing, respectively, so that increases in the wing stroke amplitudes correspond to positive changes for both sides.

Estimating the onset of wing and antennal motion. To estimate the onset of the wing and the antennal motion, we fit a line using least-squares regression through data for the mean wing and antenna angles immediately before the onset of the response and calculated its intersection with a line fit through the data during the first 10 ms of the response. Because we did not observe any responses during the first 20 ms after the start of the visual motion, we chose this period to measure the pretrial baselines. The initial response was approximately linear, and we used data points in a 10 ms window starting 25 ms after the onset of visual motion, except for left antenna angle during the RT stimulus and right antenna angle during the LT stimulus. In these two cases, there was a clear delay in the response onset, and thus data points in a 10 ms window starting 50 ms after the onset of visual motion were used instead.

Estimation of the power of the antennal oscillations at the WBF. We estimated the power of the antennal oscillations using multitaper spectral estimation procedures implemented in the Chronux toolbox (http://www.chronux.org/) (Mitra and Bokil, 2008) for MATLAB. In all analyses, we used 0.4 s time window, 5 Hz bandwidth, and three tapers. We moved the window in 50 ms steps to estimate the power of the oscillations at different time points during the trial. The power of the oscillations had a narrow peak at a frequency corresponding to WBF, and we used the maximum power for a frequency band between 150 and 250 Hz (the range of typical WBF) in each time window as the power of the antennal oscillations at WBF. Before averaging the power of the antennal oscillation at WBF, we log-transformed the data to better approximate a normal distribution.

Statistical analysis. For all experiments, we first averaged all trials under the same experimental conditions for each fly, creating a set of single time series traces. Because the data for the power of the antenna oscillation were not distributed normally, we first performed a logarithmic transformation on each data vector before averaging the data for each fly. The traces representing mean data sequences for each fly were then compared across flies and across experimental conditions using statistics toolbox in MATLAB. Unless otherwise noted, time series data are presented as a mean trace and a shaded envelope representing SEM.

Peak responses of wings, antennae, and antennal oscillations were defined as the maximum response amplitude during the 1 s period after the onset of visual motion. Baseline values were defined as the average value during the 400 ms period immediately before the onset of visual motion. We present the distributions of peak responses and baseline values using box-and-whisker plots. In these plots, the central line indicates median, the box outlines the interquartile range of the data, and the whiskers shows the range from minimum to maximum value, excluding any outliers. Outliers are defined as values that are >1.5 times the interquartile range below or above the 25th or 75th percentiles, respectively. Whenever we compared three or more experimental conditions, we used Kruskal–Wallis nonparametric one-way ANOVA, followed by a Tukey–Kramer method to find a group with a median that is significantly different from other groups. We used Wilcoxon's rank sum test for equal medians when comparing medians of two experimental conditions.

Results

Visually induced slow antennal movements are negatively correlated with ipsilateral wing stroke amplitude

To investigate how the antennae of flies move in response to visual motion, we placed rigidly tethered flies in a cylindrical electronic arena and elicited fictive turns while measuring

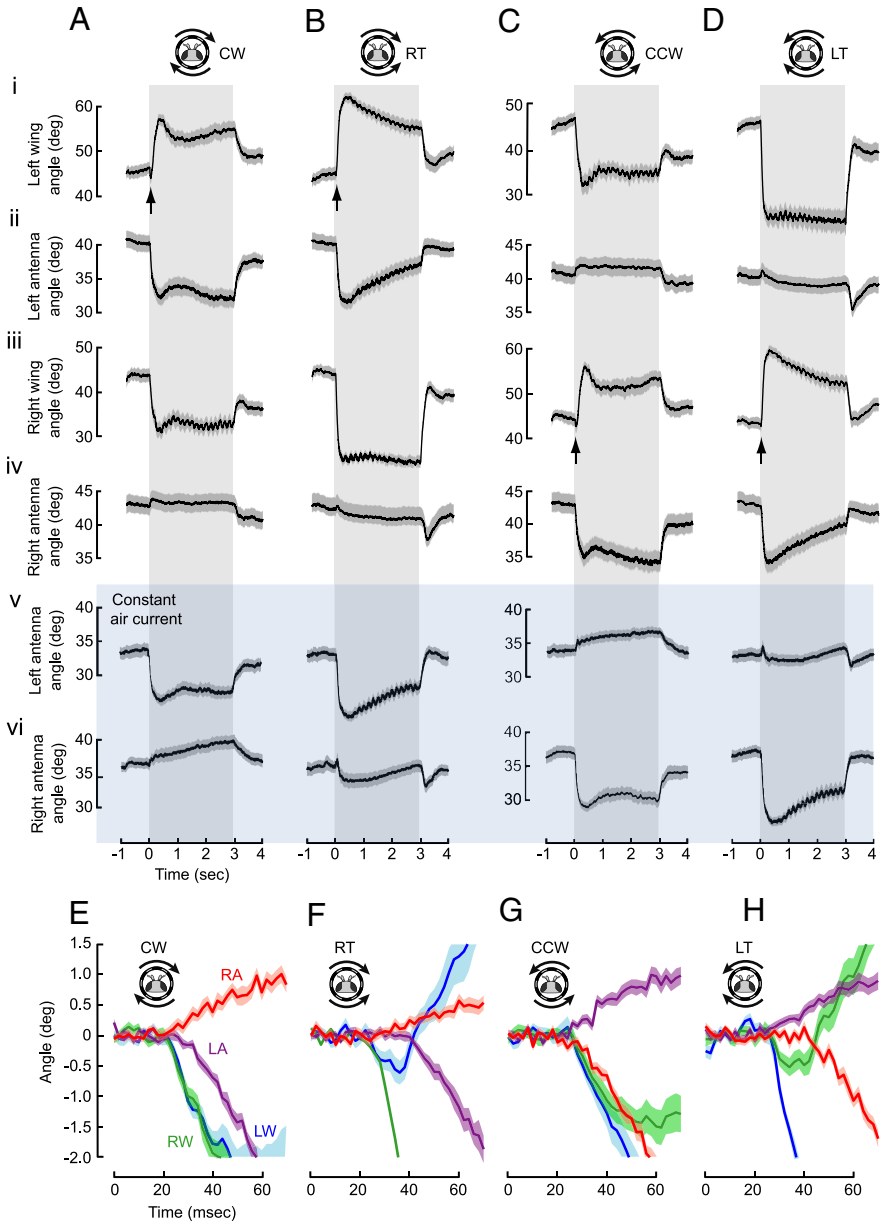

Figure 2. Antennae exhibit optomotor responses to rotational and translational visual motion. ***A–D***, Mean ± SEM angles of the left wing (***i***), left antenna (***ii***), right wing (***iii***), and right antenna (***iv***) during presentations of CW rotational (***A***, $n = 21$ flies), RT (***B***, $n = 21$ flies), CCW rotational (***C***, $n = 19$ flies), and LT (***D***, $n = 20$ flies) wide-field motion. ***v*** and ***vi*** show mean ± SEM angles of the left (***v***) and right (***vi***) antenna in response to visual motion in the presence of a constant frontal airflow (0.42 m/s; sample size for CW rotational, RT, CCW rotational, and LT visual motions were 17, 14, 18, and 17 flies, respectively). Stimulus presentation is indicated by gray shading. Pink shading indicates presence of a constant frontal airflow. In response to all stimuli, antennae moved in the direction opposite to that of the ipsilateral wing. The time course for the caudal rotation of the antenna (***Aii***, ***Bii***, ***Civ***, ***Div***) closely follows that of the changes in the ipsilateral wing stroke amplitude (***Ai***, ***Bi***, ***Ciii***, ***Diii***). Frontal airflow rotated the antennae caudally and reduced the baseline mean angles of the antennae. However, it did not significantly affect the optomotor response of antennae. Black arrows point to transient decreases in stroke amplitudes in response to the onset of visual motion. During presentations of visual motions, mean angles of the wings and antennae oscillates slightly at the temporal frequency of the visual stimuli (6.12 Hz). These oscillations are distinct from fast oscillations of antennae described in Figure 3. ***E–H***, Mean ± SEM changes in the angles of the left wing (LW; blue lines), right wing (RW; green lines), left antenna (LA; magenta lines), and right antenna (RA; red lines) from the baseline values immediately after the onset of CW rotational (***E***), RT (***F***), CCW rotational (***G***), and LT (***H***) visual motion. Wings and antennae moved near simultaneously except for the caudal rotation of the antenna in response to translational visual motion (***F***, LA; ***H***, RA). Sample size for each visual stimulus is the same as in ***A–D***.

the movements of their antennae and wings (Fig. 1*A*). Because *Drosophila* exhibit strong optomotor responses to both rotational (Götz, 1964) and translational patterns of visual motion (Tammero et al., 2004), we examined antennal motions in response to these two types of stimuli, eliciting both leftward and rightward turns. Our measurements revealed stereotyped movements of the antennae that are closely correlated with changes in wing stroke amplitude and are consistent across flies (Fig. 2*A–D*). In response to CW visual rotation, which elicits syndirectional CW turns, the left antenna rotated CCW, opposite to the direction of the visual motion. After the initial caudal rotation, the left antenna relaxed slightly forward near the middle of stimulus presentation, before once again rotating backward (Fig. 2*Aii*). This time course closely matched that for the stroke amplitude of the ipsilateral wing, although of opposite polarity (Fig. 2*Ai*). As the antennae rotated caudally, the stroke amplitude of the ipsilateral wing increased, diminishing the distance between the two appendages at ventral stroke reversal. The right antenna also rotated CCW during the CW stimulus, but the movement was much smaller compared with that of the left antenna. With CCW rotation of the visual pattern, eliciting fictive turns to the left (Fig. 2*C*), the direction of the wing and antennal optomotor responses reversed as expected of a bilaterally symmetric system.

As has been reported previously (Tammero et al., 2004), translational motion evoked stronger changes in wing stroke amplitude compared with rotational stimuli at the same contrast and temporal frequency (Fig. 2). The antennae movements in response to translational visual motion were not greater than those in responses to rotation, but they did follow a distinctly different time course. As with rotational motion, the response of the left antenna elicited by RT motion followed a time course that closely matched that of ipsilateral wing stoke amplitude, in this case an early peak followed by a constant decay (Fig. 2*Bii*). In response to the same RT stimulus, the right antenna exhibited a small transient rostral movement at the onset of visual motion and a larger caudal transient movement after the offset of visual motion (Fig. 2*Biv*). This phasic movement pattern was quite distinct from the tonic pattern elicited by rotational motion (Fig. 2*Aiv*). It is also noteworthy that the large caudal transient movement in response to translational motion long outlasted the offset of the stimulus. The responses to an LT stimulus (Fig. 2*D*) were, as expected, symmetrical with those to an RT stimulus (Fig. 2*B*).

During presentations of visual stimuli, we observed small-amplitude oscillations of wing and antenna motor responses (Fig. 2). These oscillations were more prominent during presentations of translational visual motion but were also observed during presentations of rotational motion in wings on the inside of a fictive turn. The frequency of these oscillations

matched the temporal frequency of our visual stimuli (6.12 Hz). Such effects could be explained by a sensorimotor process driven by Hassenstein–Reichardt elementary motion detectors, whose output do oscillate transiently at the temporal frequency of visual stimuli in response to the onset of the visual motion (Egelhaaf and Borst, 1989). Alternatively, such a phenomenon could also be explained by effects that have been reported for motion-sensitive interneurons in blowfly (Maddess, 1986) in which the afterimage, produced by a stationary visual pattern, interacts with moving visual patterns to modulate the output of the motion-sensitive interneurons at the temporal frequency of visual stimuli.

During free flight, the vector sum of an animal's groundspeed with the background wind would result in an airspeed that could deflect the aristae (Burkhardt and Gewecke, 1965). Because the force exerted on the aristae by air currents might influence the antennal movements we observed, we measured movements of antennae during visually induced turns in the presence of a constant frontal flow of air (Fig. 2*v–vi*). As expected, frontal air currents rotated antennae caudally and significantly reduced the baseline mean angle of the left and right antennae compared with the control cases ($p < 3.6 \times 10^{-6}$ and $p < 2.5 \times 10^{-3}$ for the left and right antenna respectively, Wilcoxon's rank sum test for equal medians). However, the visually mediated antennal motor responses were not significantly altered by the presence of the frontal airflow (Fig. 2*v–vi*, peak response amplitudes in the first second of the response were not significantly different from control cases, $p > 0.05$, Wilcoxon's rank sum test for equal medians). Because tethered flies did not fly as robustly in the presence of a constant airflow in our flight arena, all following experiments were performed in the absence of the air current.

The strong negative correlation between the motion of the ipsilateral wing and antenna during turns toward the opposite side for both rotational and translational stimuli suggests that the ipsilateral motor systems controlling these two appendages may be closely coupled by a common divergent command system. Alternatively, they might be coupled by a reflex arc in which visual stimuli elicit a motor response in one appendage (wing or antenna), which in turn activates mechanoreceptors that trigger a motor response on the other. If the coupling between motion of the ipsilateral wing and antenna were mediated by a common divergent command system, then the onset of motion at the start of the visual stimulus should be nearly synchronous for the two appendages, whereas one might expect a short delay in the case of a reflex loop. An expanded view of the mean changes in wing and antennal position from the baseline values at the onset of each trial type is shown in Figure 2*E–H*. Because the initial portion of each mean response was approximately linear, we estimated the response onset by finding the intersection between a line fit through the baseline portion of the data and a line fit through the initial response portion of the data (for details, see Materials and Methods). At the 4–5 ms temporal resolution of our measurements (stroke amplitude can only be measured on a cycle-by-cycle basis), the changes in wing stroke amplitude and antennal position appear synchronous and follow the onset of visual motion by a delay of 20–30 ms. We estimated a slightly longer visuomotor delay of 40–50 ms for the caudal antennal movement in response to translational visual motion toward the contralateral side. Although these measurements do not rule out the possibility that optomotor responses of the wing and antenna are correlated as a result of a mechanosensory reflex arc, as opposed to divergent or parallel visuomotor pathways, we found no evidence for a delay of one motor system relative to the other.

The expanded timescale in Figure 2*E–H* indicates an unexpected feature of the optomotor responses of the wing. For all patterns of visual motion, both wings exhibited an initial decrease in stroke amplitude in response to visual motion. This was true not only for the inside wing, which is expected to exhibit a steady-state decrease in stroke amplitude, but also for the wing on the outside of a turn that eventually exhibits an increase in stroke amplitude. These brief small-stroke amplitude transients are readily visible in the contracted time series data of Figure 2*A–D* (arrows) and last ~100 and 20 ms for rotational and translational stimuli, respectively. To our knowledge, these brief transients in wing motions have not been reported before, despite the extensive previous analysis of these optomotor reflexes. The antennae, in contrast, do not exhibit these reversals in motion at the onset of the visual stimulus (Fig. 2*E–H*).

As discussed above, we observed a strong correlation between the average traces for antennal position and ipsilateral wing stroke amplitude during visually elicited turns toward the opposite side. To test whether these correlations were present on a trial-by-trial basis, we calculated the cross-correlation between the antennal position and the wing stroke amplitude during the turning responses for each trial. For all stimuli, mean correlation coefficients were negative and peaked at a time lag of −2 ms, which is less than the time resolution of our measurements of wing stroke amplitude. These measurements indicate that the wing and ipsilateral antenna moved nearly synchronously (albeit in opposite directions) at the onset of visual motion.

To test whether the antenna movements we measured were specific to flight behavior, we presented the identical visual patterns to tethered flies that were not flying. Under these conditions, the average movements in response to both rotational and translational stimuli were all <1° (data not shown). Although these small movements of the antennae in non-flying flies may have some functional significance, they do not resemble the antennal movements of flying flies in either magnitude or pattern of motion. Thus, the optomotor reflexes of the antenna shown in Figure 2 are qualitatively gated by flight behavior.

Antennae oscillate at WBF during flight

In addition to the tonic movements of the antennae in response to visual motion and the small-amplitude oscillations at the temporal frequency of the visual stimuli, we also observed that the antennae oscillated rapidly at the frequency of the wing beat and that the amplitude of this oscillation increased during turning responses as the antenna moved caudally toward the stroke envelope of the ipsilateral wing (Fig. 3). Figure 3*A* shows an example record of the left antenna position from a trial in which a fly was presented with CW rotational motion. As can be seen in the expanded records before and during the turning response (Fig. 3*Ai*,*Aii*), fast oscillation of the left antenna increased substantially during the presentation of the rotational motion and persisted afterward. A spectrogram of antennal position for this trial shows a distinct ridge throughout stimulus presentation at a frequency that corresponds precisely to that of the wing beat (Fig. 3*B*). In addition, the spectrogram exhibits sharp peaks in power at time periods that correspond to caudal rotations of the antenna and simultaneous increases in the left wing stroke amplitudes (Fig. 3*A*). One limitation of our measurement technique, based on machine vision, is that we could only sample antennal position at 500 Hz, which is just below the Nyquist limit for the WBF (~200 Hz). To confirm that the fast oscillations of the antennae were indeed synchronized with the wing beat, we used a high-speed video camera to record the motion of the wings and antennae at 6000 frame/s (data not shown). These movies show that the antenna starts to rotate caudally during the ventral reversal of the

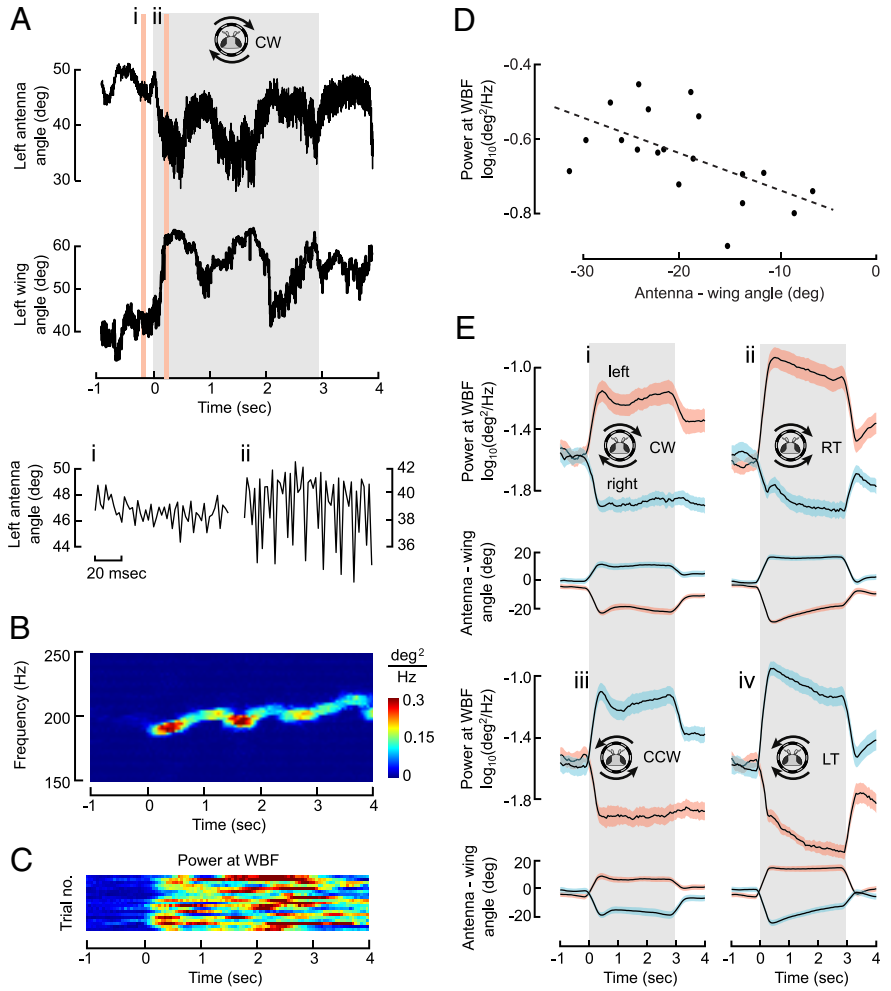

Figure 3. Antennae oscillate passively at WBF and the amplitude of oscillation increases during turning responses. ***A***, An example trace of the left antenna and left wing angles during a presentation of a CW rotational visual motion. Expanded views of regions shaded by pink before and during the presentation of the visual motion are shown in ***Ai*** and ***Aii***, respectively. The oscillation of the antenna increased greatly when the antenna approaches the wing stroke envelope during the turning response. ***B***, A spectrogram showing the changes in power of the left antenna oscillations during the trial shown in ***A***. The power of the oscillation peaked at a narrow frequency range that corresponds to WBF, and the power increased when the gap between the wing and the antenna narrowed. ***C***, The power of the left antenna oscillations at WBF at different time points during 19 trials in which a fly was presented with CW rotational visual motion. The power of the oscillations increased consistently during the presentation of the stimulus (0–2.94 s). ***D***, The peak power of the left antenna oscillations at WBF (shown as $\log_{10}$ of the power) for the trials shown in ***C*** plotted against the difference between the angles of the left antenna and the wing at that time point. The peak power of the oscillation for each trial was negatively correlated with the angular distance between the antenna and the wing ($r = -0.5543$, $p < 1.38 \times 10^{-2}$). The black dotted line indicates linear regression line. ***E***, The mean ± SEM power of the antenna oscillations at WBF (shown as $\log_{10}$ of the power) and the mean ± SEM difference between the angles of the antenna and the wing (left side, pink shade; right side, blue shade) during the presentations of CW rotational (***i***), RT (***ii***), CCW rotational (***iii***), and LT (***iv***) visual motion (areas shaded by light gray). In response to all patterns of visual motion, the oscillations of the antenna that rotated caudally (left side for ***i*** and ***ii***; right side for ***iii*** and ***iv***) increased while the oscillations of antenna that rotated rostrally (right side for ***i*** and ***ii***; left side for ***iii*** and ***iv***) decreased. Time course for the increase in the power of the antennal oscillation was similar to that for the difference in the angles of that antenna and the ipsilateral wing. Sample size for each visual stimulus is the same as in Figure 2.

wing stroke, just as the wing starts to move backward at the start of the upstroke. This observation suggests that the air currents induced by the motion of the wings can drive an oscillation of the antennae, which is consistent with previous reports in other insects (Gewecke and Schlegel, 1970; Sane et al., 2007). Although small mechanical vibrations of the body might also cause the antenna to oscillate, experiments described later in which we remove a large portion of the wing argue against this interpretation.

The observation that fast antennal oscillation increased during turning responses was consistent across trials (Fig. 3*C*). In all cases, it was the antenna that rotated caudally, moving closer to the ventral reversal point of the ipsilateral wing, that exhibited the increase in oscillation power. Figure 3*C* shows the time course of power at WBF for the left antenna during 19 trials in which we presented a fly with a CW rotating visual pattern. The power at WBF consistently increased during the turning response. To investigate whether the trial-to-trial variability in the power at WBF was correlated with the distance between the wing and antenna during the trial, we plotted peak power at WBF during each trial shown in Figure 3*C* against the angular distance between the wing and antenna at that time point (Fig. 3*D*). We found a significant negative correlation between these two variables (Fig. 3*D*) ($r = -0.5543$, $p < 1.38 \times 10^{-2}$), providing additional evidence that antennal oscillations increase when the antenna moves closer to the ipsilateral wing.

The antenna that rotated caudally during the turning response increased in oscillation amplitude consistently across flies and across different visual stimuli (Fig. 3*E*). Translational motion, which evoked stronger turning responses, also caused larger increase in antennal oscillation (Fig. 3*E*). With all visual stimuli, power at WBF increased when the difference between the antenna angle and the wing angle decreased (Fig. 3*E*). The antenna that rotated rostrally during turning responses (away from the stroke reversal point of its ipsilateral wing) consistently exhibited a decrease in oscillation amplitude (Fig. 3*E*). All these observations are consistent with the hypothesis that induced air currents are the cause of the antennal oscillation.

We also tested whether a presence of a constant frontal flow of air affects the antennal oscillation at WBF. Constant airflow decreased the antennal oscillation during the baseline period before the presentation of visual motion ($p < 6.25 \times 10^{-9}$ and 2.15×10^{-9} for the left and right antenna, respectively, Wilcoxon's rank sum test for equal medians) (data not shown). This decrease may indicate that the PF joint is stiffened when the arista is pushed caudally by the airflow. The power of the antennal oscillation still increased significantly when the angular distance between the antenna and the ipsilateral wing decreased during the visually induced turns ($p < 2.93 \times 10^{-4}$, 1.22×10^{-4}, 5.36×10^{-4}, and 2.93×10^{-4} for CW, RT, CCW, and LT visual motion, respectively; Wilcoxon's signed rank test for zero median) (data not shown), but it increased less than the control cases for the CCW and LT visual motion ($p < 8.76 \times 10^{-4}$ and 1.09×10^{-2} for CCW and LT visual motion, respectively, Wilcoxon's rank sum test for equal medians) (data not shown). For all visual mo-

tion, the power of the antennal oscillation decreased significantly when the angular distance between the antenna and the ipsilateral wing envelope increased during visually induced turns ($p < 2.3 \times 10^{-3}$, 3.1×10^{-3}, 3.27×10^{-4}, and 7.12×10^{-4} for CW, RT, CCW, and LT visual motion, respectively, Wilcoxon's signed rank test for zero median) (data not shown), although this decrease was smaller than in control cases ($p < 2.36 \times 10^{-5}$, 2.3×10^{-2}, 9.81×10^{-6}, and 7.58×10^{-4} for CW, RT, CCW, and LT visual motion, respectively, Wilcoxon's rank sum test for equal medians) (data not shown). These results suggest that, although a constant airflow decreases the power of the antennal oscillation, it does not affect the basic finding that this passive oscillation is inversely correlated with the angular distance between the antenna and the ipsilateral wing envelope.

Slow large movements of the antennae are primarily attributable to rotation of the SP joint, whereas fast antennal oscillations are attributable to rotation of the PF joint

Although the time course and magnitude of the antennal movements during visually elicited turns suggest that active movements of the SP joint are responsible for the slow large movements of the antennae and the passive deflections of the PF joint are responsible for the fast oscillations, our tracking algorithm does not allow us to directly confirm this. Our method measures only the angle of the arista relative to the horizontal plane of the image, but this angle is altered by rotation of both the SP joint and the PF joint. To identify the joint movements that are responsible for each type of antennal movement, we physically restricted the motion of either the SP joint or the PF joint and measured the effects of such manipulations on antennal motion. These experiments also allowed us to investigate possible functional roles of each joint movement during visually induced turns by measuring the effect on the wing motion.

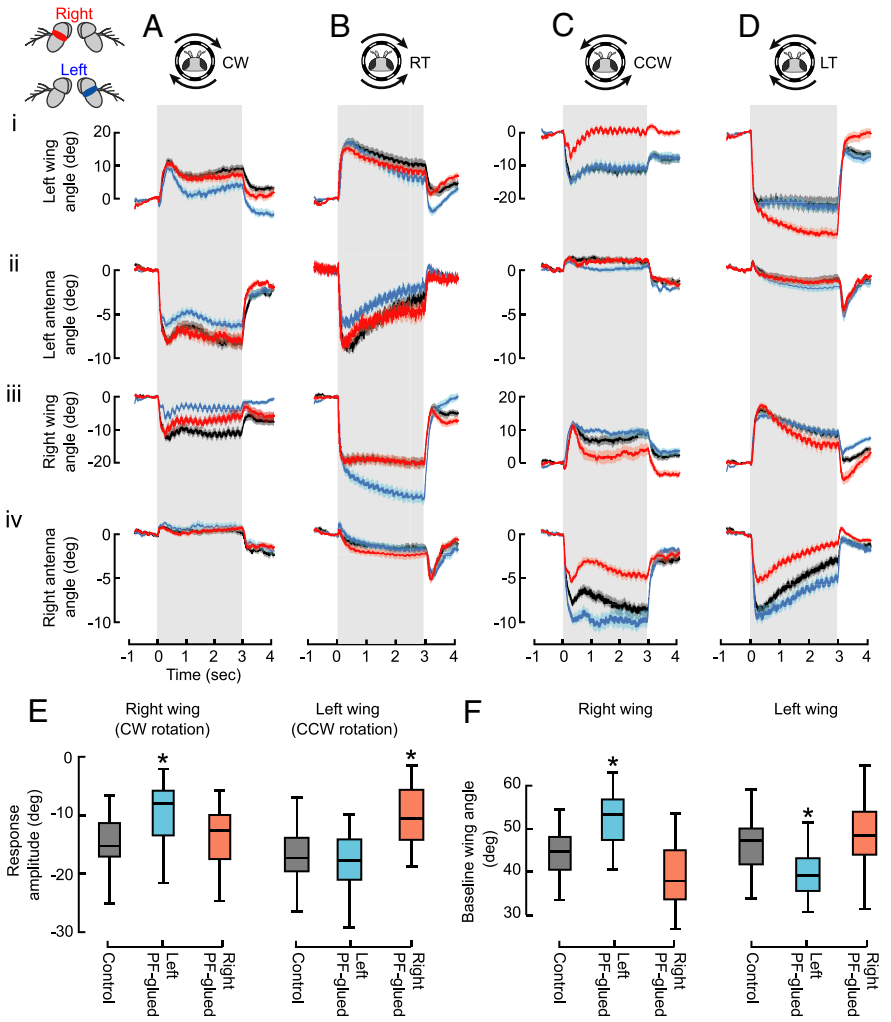

Figure 4. Blocking the passive movements of the PF joint slightly decreases the caudal rotation of the antenna and alters the optomotor responses of the wings. ***A–D***, Mean ± SEM changes in the angles of the left wing (***i***), left antenna (***ii***), right wing (***iii***), and right antenna (***iv***) during presentations of CW rotational (***A***), RT (***B***), CCW rotational (***C***), and LT (***D***) visual motion (areas shaded with light gray), in control (black), right PF-glued (red), and left PF-glued (blue) flies. Control data are from the same experiments as shown in Figure 2. For the right PF-glued flies, sample size for CW rotational, RT, CCW rotational, and LT visual motions were 23, 23, 23, and 25, respectively. For the left PF-glued flies, sample sizes were 25, 26, 24, and 28, respectively. The caudal rotation of the antenna (***Aii***, ***Bii***, ***Civ***, ***Div***) decreased slightly when the PF joint was glued. During presentations of rotational visual motions, interfering with JO function reduced the decrease in the contralateral wing stroke amplitude (***Aiii***, ***Ci***) and slowly reduced the increase in the ipsilateral wing stroke amplitude (***Ai***, ***Ciii***). In contrast, during presentations of translational visual motions, JO interference slowly increased the decrease in the contralateral wing stroke amplitude (***Biii***, ***Di***). ***E***, Box-and-whisker plots (for details, see Material and Methods) showing the distributions of the peak response amplitudes of the right wing during CW rotational visual motion and the left wing during CCW rotational visual motion in control, left PF-glued, and right PF-glued flies. In response to rotational visual stimuli, stroke amplitude decreased significantly less when the contralateral antenna was glued. ***F***, Box-and-whisker plots showing the distributions of the baseline wing angles for the left and right wings in control, left PF-glued, and right PF-glued flies. Interfering with the left JO significantly increased the baseline right wing angle and decreased the baseline left wing angle. Asterisks indicate a group with a median that is significantly different from the others ($p < 0.05$, Tukey–Kramer *post hoc* comparison of the medians).

In the first set of experiments, we restricted the movement of the PF joint in one antenna by gluing it with UV-cured glue and measured the motion of the antennae and the wing in response to visual stimuli (Fig. 4). This allowed us to measure the active movements of the SP joint in the absence of the passive movements of the PF joint. To show the effect of the gluing of the PF joint on the turning responses more clearly, we have plotted changes in antennal position and wing stroke amplitude after subtracting the mean angular position before the onset of the visual stimulus (Fig. 4). The slow large movements of the antennae in response to visual motion were essentially intact even when the PF joint was fixed with glue, suggesting that active movements of the SP joint are indeed responsible for the majority of this antennal motion (Fig. 4*A–D*). However, fixing the PF joint did result in small but significant changes in the amplitude of the slow antennal movements. For CW rotation and the RT stimulus, the left antenna rotated significantly less caudally when its PF joint was glued compared with unglued controls, or the right PF-glued flies ($p < 8.87 \times 10^{-3}$ and $p < 2.19 \times 10^{-3}$, respectively, Tukey–Kramer *post hoc* comparison of the medians). The results were similar for the rotation of the right antenna during CCW rotation and the LT stimulus ($p < 1.49 \times 10^{-4}$ and $p < 5.65 \times 10^{-5}$, respectively, Tukey–Kramer *post hoc* comparison

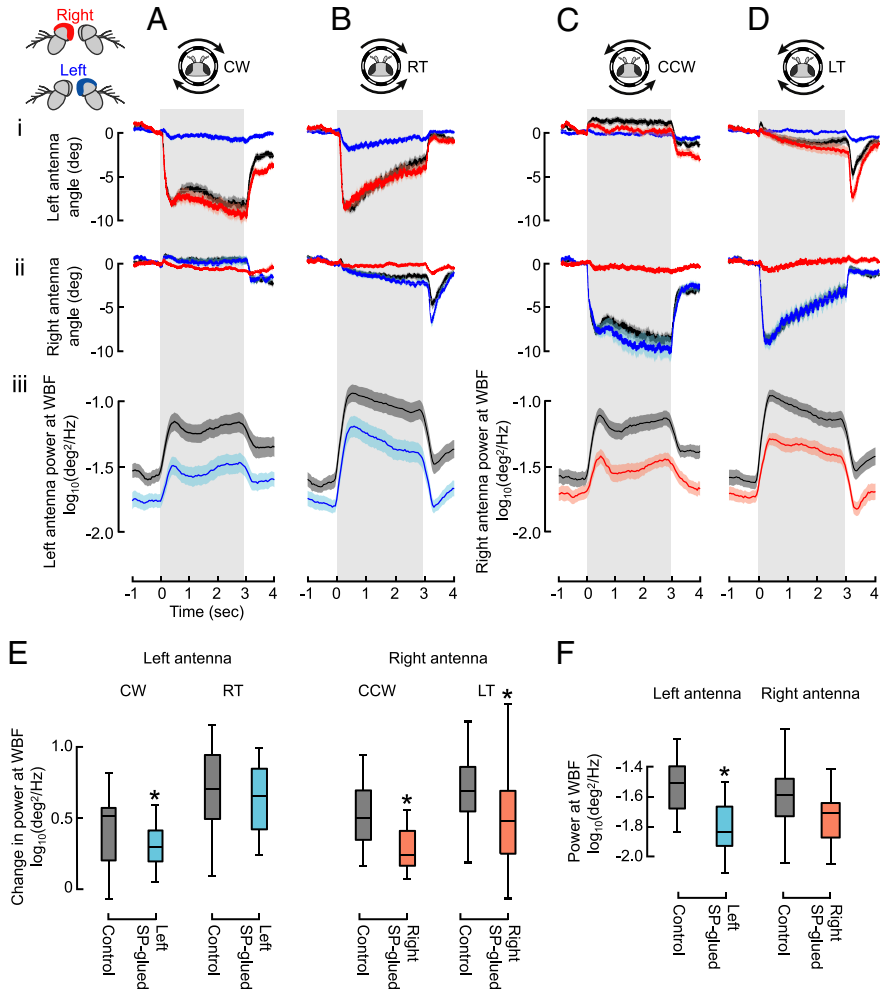

Figure 5. Blocking the active movement of the SP joint greatly reduces the slow antennal motion and decreases the increase in the antennal oscillation. ***A–D***, Mean ± SEM changes in the angles of the left (***i***) and right (***ii***) antenna and the mean ± SEM power of the oscillation at WBF (shown as $\log_{10}$ of the power) for the antenna that rotated caudally (***iii***) during presentations of CW rotational (***A***), RT (***B***), CCW rotational (***C***), and LT (***D***) visual motion (areas shaded with light gray), in control (black), the right SP-glued (red), and the left SP-glued (blue) flies. Control data are from the same experiments as shown in Figure 2. For the right SP-glued flies, sample sizes for CW rotational, RT, CCW rotational, and LT visual motions were 18, 20, 19, and 20, respectively. For the left SP-glued flies, sample sizes were 19, 19, 18, and 19, respectively. Gluing the SP joint greatly reduced but did not completely eliminate the slow antennal motions (***i***, ***ii***). The power of the antennal oscillation increased less during visually induced turns when the SP joint was glued (***iii***). ***E***, Box-and-whisker plots showing the distributions of the peak changes in the power of the antennal oscillations at WBF (shown as $\log_{10}$ of the power) during presentations of CW rotational, RT, CCW rotational, and LT visual motion for the control (black), the left SP-glued (blue), and the right SP-glued (red) flies. For each pattern of visual motion, only the antenna on the side that normally shows a caudal rotation is shown (i.e., left side for CW rotational and RT motion, right side for CCW rotational and LT motion). Asterisks indicate a median that is significantly different from the control ($p < 0.05$, Wilcoxon's rank sum test for equal medians). For all stimuli except RT motion, blocking the active caudal rotation of the antenna by gluing the SP joint significantly reduced the increase in the power of the antennal oscillations. ***F***, Box-and-whisker plots showing the distributions of the baseline power of the antennal oscillation (shown as $\log_{10}$ of the power) for the left and right antenna for the control (black), the left SP-glued (blue), and the right SP-glued (red) flies. Asterisks indicate a median that is significantly different from the control ($p < 0.05$, Wilcoxon's rank sum test for equal medians). Gluing the SP joint significantly reduced the baseline power of the antennal oscillation for the left antenna.

of the medians). These decreases in the antennal optomotor response might be caused by the lack of feedback from the mechanosensory neurons that respond to the movements of the PF joint or, alternatively, could indicate that the small portion of the slow large movements of the antennae is attributable to a slight passive deflection of the PF joint as discussed below (Fig. 5).

In contrast to the small effect it had on the large slow movements of the antennae, gluing the PF joint greatly reduced the fast small oscillations of the antennae at WBF compared with the controls ($\log_{10}$ of mean ± SEM power at WBF decreased from −1.562 ± 0.0493 and −1.598 ± 0.0517 deg^2/Hz to −2.333 ± 0.0230 and −2.240 ± 0.0249 deg^2/Hz for the left and right PF-glued flies respectively; $p < 6.15 \times 10^{-13}$ and $p < 8.64 \times 10^{-12}$ for the left and right PF-glued flies, respectively, Wilcoxon's rank sum test for equal medians). Furthermore, the power of the fast antennal oscillations did not increase in PF-glued flies even when the wing and the antenna came closer together during the visually induced turning responses ($\log_{10}$ of mean ± SEM power at WBF very slightly decreased by 0.032 ± 0.012, 0.038 ± 0.010, 0.027 ± 0.012, and 0.027 ± 0.012 deg^2/Hz for CW, RT, CCW, and LT visual motion, respectively; this decrease was statistically significant for CW and RT visual motion, $p < 1.6 \times 10^{-3}$ and $p < 1.7 \times 10^{-3}$, but not significant for CCW and LT visual motion, $p > 0.05$, Wilcoxon's signed rank test for zero median). These results support our hypothesis that the antennal oscillations at WBF represent passive movement of the PF joint.

In all cases, there were no significant differences in the antennal motor responses of control flies and those in which the contralateral PF joint was glued, suggesting that any influence of the manipulation on antennal motion acts ipsilaterally. Gluing the PF joint also slightly shifted the mean baseline position of the antenna in the absence of visual motion (data not shown), but none of the changes were statistically significant ($p > 0.05$, Kruskal–Wallis one-way ANOVA).

Interfering with JO function decreases optomotor responses of wings in response to rotational visual motion

Blocking the movement of the PF joint interferes with the function of the JO located in the pedicel (Johnston, 1855). The JO is the major mechanosensory organ of the antenna, consisting of ~200 scolopidia and their associated neurons (Caldwell and Eberl, 2002) and encodes movement of the PF joint (Ewing, 1978; Eberl et al., 2000; Kamikouchi et al., 2009; Yorozu et al., 2009). Because the JO is a major, but not exclusive, source of the mechanosensory feedback from the antenna, this manipulation allowed us to investigate whether mechanosensory information from the antennae is used to modulate the motion of wings during turning responses.

Interfering with JO function by gluing the PF joint in one antenna caused several changes in wing motion, suggesting that mechanosensory feedback from the antennae does indeed modulate wing motion (Fig. 4). During turning responses to rotational stimuli, the inside wing normally exhibits a drop in stroke

amplitude, but this decrease was greatly diminished when the PF joint of the contralateral antenna was glued (Fig. 4*Aiii*,*Ci*). For example, when the left PF joint was glued, the right stroke amplitude decreased significantly less in response to CW rotation compared with both controls and the right PF-glued flies ($p < 1.85 \times 10^{-2}$, Tukey–Kramer *post hoc* comparison of the medians) (Fig. 4*E*). Similarly, in response to CCW rotation, left stroke amplitude decreased significantly less when the right PF joint was glued compared with the control and the left PF-glued flies ($p < 9.00 \times 10^{-4}$, Tukey–Kramer *post hoc* comparison of the medians) (Fig. 4*E*). We also observed a change in the response of the ipsilateral wing with the gluing of the PF joint, although the effect was more subtle. The increase in stroke amplitude at the onset of visual motion was identical to controls and contralateral PF joint manipulations, but after ~300 ms, the response decreased to a much lower steady-state value (Fig. 4*Ai*,*Ciii*). If stroke amplitude is correlated with yaw torque as has been documented in several previous studies (Götz et al., 1979; Tammero et al., 2004), the above two effects would both decrease the compensatory torque response to a rotational visual stimulus, suggesting that the mechanosensory feedback mediated by JO afferents normally increases the strength of optomotor responses to rotational visual motion.

Curiously, the effect of gluing the PF joint was quite different for the changes in wing stroke amplitude induced by translational visual motion. In particular, instead of a diminished drop in stroke amplitude, the inside wing exhibited a larger response to the stimulus (Fig. 4*Biii*,*Di*). This increased response only emerged after ~200 ms, and the response continued to increase slowly throughout the 3 s presentation of visual motion.

In addition to the effects of JO interference on the responses to visual motion, we also observed a bilateral effect on the baseline mean stroke amplitude when the visual display was stationary. The baseline stroke amplitude of the wing ipsilateral to the glued PF joint decreased, whereas the stroke amplitude of the wing contralateral to the glued PF joint increased (Fig. 4*F*). This asymmetry suggests that a fly would turn toward the side of the glued PF joint in the absence of visual motion. This tendency to turn toward the side of the manipulated antenna (and away from the intact side) is consistent with the influence of JO interference on upwind orientation responses (Budick et al., 2007) but is opposite to the effect of the same manipulation on olfactory-mediated turns (Duistermars et al., 2009), suggesting that JO-mediated mechanosensory reflexes may play different roles depending on the behavior. Interestingly, this effect was larger for manipulations of the left JO than for the right JO, confirming previous observations of bilateral asymmetries in antenna-mediated reflexes (Duistermars et al., 2009). For the right wing, flies with their left PF joint glued had significantly higher median stroke amplitude compared with both the controls and the right PF joint glued flies ($p < 2.5 \times 10^{-3}$, Turkey–Kramer *post hoc* comparison of the medians) (Fig. 4*F*). Although gluing the right PF joint produced a trend of decreasing the stroke amplitude of the right wing, the effect was not statistically significant at the $p = 0.05$ level (Tukey–Kramer *post hoc* comparison of the medians) (Fig. 4*F*). A similar pattern was observed for the left wing as well, i.e., the effect of gluing the right PF joint did not generate as strong an effect as gluing the left. Flies with their left PF joint glued had significantly lower median wing stroke amplitudes compared with both the controls and the right PF-joint-glued flies ($p < 0.037$, Turkey–Kramer *post hoc* comparison of the medians) (Fig. 4*F*). Flies with their right PF joint glued exhibited a slight trend of increased wing stroke amplitude compared with the controls, but this trend was not statistically significant ($p > 0.05$, Tukey–Kramer *post hoc* comparison of the medians) (Fig. 4*F*). However, when compared within the right PF-joint-glued flies, the combined effect of increasing the left wing stroke amplitude and decreasing the right wing stroke amplitude was large enough that the median angle for the left and the right wing was significantly different ($p < 1.67 \times 10^{-4}$, Wilcoxon's rank sum test for equal medians). Collectively, these data suggest that, in the absence of visual motion, mechanosensory afferents of the JO act to increase amplitude on the ipsilateral wing and decrease amplitude on the contralateral wing and that this pathway is measurably stronger for the left JO than the right. We do not believe that this laterality was attributable to uneven gluing of one PF joint relative to the other caused by the experimenter's handedness, because we performed control experiments in which the PF joint was glued by right- and left-handed members of the laboratory. Both datasets showed a similar trend in laterality (data not shown).

The PF joint moves tonically by a small amount during visually induced turns

Antennal movements of the flies with their PF joints glued suggest that, although the movement of the SP joint is mainly responsible for the large slow motion of the antenna, the PF joint may also move tonically by a small amount during the visually induced turns. To test this hypothesis, we glued the SP joints of the flies and tested whether their antennae still showed some small tonic deflection during visually induced turns (Fig. 5*i*,*ii*). Consistent with the above hypothesis, gluing the SP joint greatly reduced, but did not completely eliminate, the slow antennal movements (Fig. 5*i*,*ii*). As shown in Figure 2, an intact antenna rotates caudally during presentation of visual stimuli that elicit fictive turns to the opposite side. Even when their SP joint was glued, antennae exhibited a small but significant caudal rotation, although greatly reduced in magnitude compared with the intact case (Fig. 5*Ai*,*Bi*,*Cii*,*Dii*). To investigate whether these residual movements were attributable to the incomplete gluing of the SP joint, we visually inspected our videos but could not detect any movements of the pedicel relative to the scape. Instead, we observed that the funiculus and the arista were rotating relative to the fixed pedicel, suggesting that these residual movements are caused by the movements of the PF joint and not the incomplete gluing of the SP joint. We know of no means by which the fly can directly actuate the PF joint by muscles, because the two intrinsic muscles of the antenna are positioned so as to actuate the SP joint (Hartenstein, 2006), although such movement might be possible by controlling the flow of hemolymph within the head capsule. A more likely explanation is that the PF joint is tonically deflected caudally by the induced airflow created by the ipsilateral wing, which strengthens as stroke amplitude increases. According to this hypothesis, the flow field generated by the wings subjects the aristae to both an oscillation (Fig. 3) as well as a small tonic caudal deflection, a view that is entirely consistent with detailed measurements of the flow field generated by flapping wings of *Drosophila* (Dickinson and Götz, 1996; Poelma et al., 2006). Because air is accelerated downward by the wings, the pressure is on average lower in the column of induced air, conditions that are expected to generate a caudal deflection of the arista. The caudal deflection of an SP-glued antenna is particularly prominent during responses to translational motion (Fig. 5*Bi*,*Dii*). This is consistent with the above model because the rostral advance of the ipsilateral stroke amplitude is particularly large in these cases.

The antenna on the inside of a fictive turn typically exhibits a small rostral movement in response to visual motion (Fig. 2). In

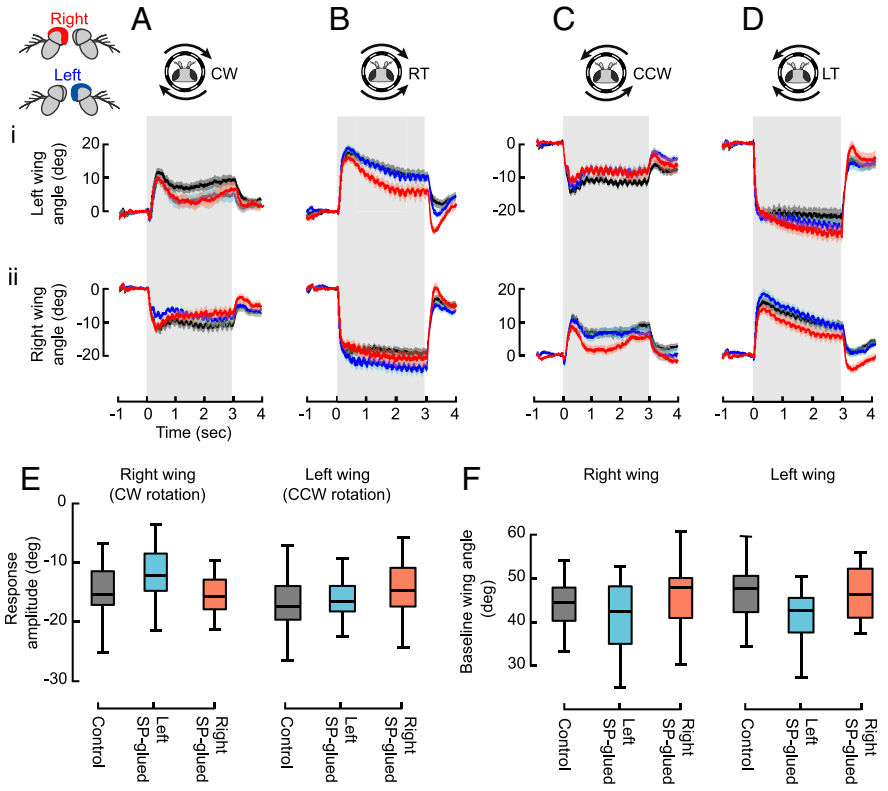

Figure 6. Blocking the active movements of the antennae by gluing the SP joint does not significantly affect the motion of the wings. ***A–D***, Mean ± SEM changes in the angles of the left (***i***) and right (***ii***) wing during the presentations of CW rotational (***A***), RT (***B***), CCW rotational (***C***), and LT (***D***) visual motion (areas shaded with light gray), in control (black), the right SP-glued (red), and the left SP-glued (blue) flies. Sample size for control and SP-glued flies are the same as in Figures 2 and 5, respectively. Gluing the SP joint did not significantly affect the motion of the wings in response to visual stimulation. ***E***, Box-and-whisker plots showing the distributions of the peak response amplitudes of the right wings during CW rotational visual motion and the left wings during CCW rotational visual motion for control, the left SP-glued (blue), and the right SP-glued (red) flies. The medians for all groups were not statistically significantly different ($p < 0.05$, Tukey–Kramer *post hoc* comparison of the medians). ***F***, Box-and-whisker plots showing the distributions of the baseline right and left wing angles for control, the left SP-glued (blue), and the right SP-glued (red) flies. The medians for all groups were not statistically significantly different ($p < 0.05$, Tukey–Kramer *post hoc* comparison of the medians).

this case, the motion is almost completely abolished by gluing the SP joint (Fig. 5*Aii*,*Bii*,*Ci*,*Di*). However, we did observe a small residual rostral transient at the onset of visual motion. The presence of this transient is also consistent with a model in which the motion is attributable to changes in the induced flow field of the flapping wings. As noted in the discussion of Figure 2, the onset of visual motion is marked by a transient decrease in stroke amplitude of both wings, even the wing on the outside of a fictive turn that will eventually exhibit an increase in amplitude. This brief drop in stroke amplitude, which reduces the strength of the induced flow field at the antenna, might explain the brief rostral motion of the arista when the SP joint is fixed.

Active movements of the antenna increase the amplitude of the antennal oscillations

Blocking the movements of the SP joint also allowed us to test whether active antennal movements contribute to the changes in the magnitude of the antennal oscillations at WBF observed during visually induced turns. Because the magnitude of the oscillation increases as the angular distance between the wing and the antenna decreases (Fig. 3), active movements of the SP joint might influence the wing-induced antennal motion. Consistent with this hypothesis, gluing the SP joint of an antenna reduced the increase in oscillation accompanying the turning responses (Fig. 5*iii*). When the SP joint was glued, the antennal oscillation for the left antenna increased significantly less than control flies in response to CW rotation ($p < 4.5 \times 10^{-2}$, Wilcoxon's rank sum test for equal medians) (Fig. 5*E*). The oscillation also increased less in response to the RT stimulus, but this effect was not statistically significant ($p > 0.05$, Wilcoxon's rank sum test for equal medians) (Fig. 5*E*). For the right antenna, oscillation increased significantly less in response to both the CCW rotation and the LT stimulus ($p < 9.4 \times 10^{-3}$ and 1.67×10^{-2}, respectively, Wilcoxon's rank sum test for equal medians) (Fig. 5*E*). These results suggest that the active slow movements of the SP joint play a significant role in increasing the oscillation at WBF by bringing the antenna and the wing closer together. However, because inhibiting the movements of the SP joint did not completely abolish the increase in oscillation, it is likely that the rostral advance of the wing stroke envelope plays the dominant role in actively coupling wing and antennal motion. This effect might also explain the reduction of the increase in antennal oscillation during visually induced turns when the SP joint is fixed with glue. However, ipsilateral wing stroke amplitude was not affected in these flies as discussed below (Fig. 6).

We also observed a small, but significant, decrease in the power of baseline oscillation for the left antennae when we glued its SP joint ($p < 1.1 \times 10^{-3}$, Wilcoxon's rank sum test for equal medians) (Fig. 5*F*). Gluing the SP joint of the right antenna also decreased its baseline power of oscillation, but this effect was not statistically significant ($p > 0.05$, Wilcoxon's rank sum test for equal medians) (Fig. 5*F*). These effects on the baseline oscillation are probably attributable to the fact that we could not fix the position of the antenna perfectly in its normal flight position during the gluing procedure, possibly placing it in a slightly more rostral location, farther from the wing stroke envelope (for details, see Materials and Methods).

Active antennal movements do not significantly alter visually induced turns

Gluing the SP joint also allowed us to test whether active movements of this joint have any functional effect on wing motion during visually induced turns (Fig. 6). Results from experiments in which we glued the PF joint suggest that JO-mediated mechanosensory input plays a significant role in determining wing motion during visually induced turns (Fig. 4). However, from such experiments, it is not possible to determine what type of antennal motion is activating the JO neurons that are responsible for changing wing motion. The active movements of the SP joint might alter the input to the JO by enhancing the increase in the amplitude of the fast antennal oscillations (Fig. 5) or, alternatively, by generating a transient inertial displacement of the funiculus relative to the pedicel when the base of the antenna is

accelerated. If either of these effects are detected by JO neurons and used to regulate wing motion, then blocking the movements of the SP joint should alter wing kinematics during visually induced turns. However, gluing the SP joint did not significantly alter the visually induced turning responses of the wings, suggesting that, in tethered head-fixed flies at least, active movements of the SP joint do not significantly change the activity of JO neurons that are responsible for altering wing motion. For rotational visual motion, gluing the SP joint did not change the peak steering responses of the wing significantly ($p > 0.05$, Tukey–Kramer *post hoc* comparison of the medians) (Fig. 6*E*), although there was a slight decrease in the responses that developed later, for both the wings on the inside and outside of fictive turns (Fig. 6*Ai*,*Aii*,*Ci*,*Cii*). The situation for translational visual stimuli was similar in that blocking the active motion of the antennae did not change the steering response of the wing significantly ($p > 0.05$, Tukey–Kramer *post hoc* comparison of the medians), although it slightly augmented the decrease in stroke amplitude on the inside wing during the latter half of the response when the contralateral SP joint was glued (Fig. 6*Bii*,*Di*). We found no statistically significant influence of gluing the base of the antenna on the mean stroke amplitude during the 400 ms before the start of visual motion ($p > 0.05$, Tukey–Kramer *post hoc* comparison of the medians) (Fig. 6*F*). These results suggest that JO neurons responsible for enhancing the turning responses are activated by at least one of the two types of changes in antennal motion still present in the SP joint glued flies: the residual increase in the magnitude of antennal oscillations at WBF (Fig. 5*iii*) and the small caudal rotation of the funiculus (Fig. 5*Ai*,*Bi*,*Cii*,*Dii*).

Reducing wing-induced air currents significantly alters antennal oscillation at WBF but leaves the slow antennal movements intact

If wing-induced air currents are responsible for the antennal oscillation at WBF and active movements of the SP joint are primarily responsible for the slow antennal motion, then reducing the wing-induced flows should alter the fast oscillation but leave the slow motion intact. To test this prediction, we reduced the wing-induced air currents on one side of the fly by cutting off approximately two-thirds of the wing (for details, see Materials and Methods) and measured the effect on antennal motions during visually induced turns (Fig. 7*i–iv*). When the wing-induced air currents were reduced by this procedure, the slow antennal motions during visually induced turns remained similar to control conditions, except that the antenna rotated slightly less caudally (Fig. 7*i*,*ii*). Compared with the control cases, left antennae rotated less caudally in response to CW and RT visual motion when left wings were cut ($p < 9.84 \times 10^{-3}$ and $p < 2.74 \times 10^{-2}$ for CW and RT motions, respectively, Tukey–Kramer *post hoc* comparison of the medians), and right antennae rotated less caudally in response to CCW and LT motions when right wings were cut ($p < 9.81 \times 10^{-4}$ and $p < 2.95 \times 10^{-2}$ for CCW and LT motions, respectively, Tukey–Kramer *post hoc* comparison of the medians). These results further support the hypothesis that the slow antennal motion in response to visual stimuli is composed of a large active movement of the SP joint and a small tonic deflection of the PF joint generated by wing-induced airflow. Cutting wings did not significantly affect the rostral rotation of the antenna ($p > 0.05$, Tukey–Kramer *post hoc* comparison of the medians), except that the right antenna rotated slightly more rostrally in response to RT motion when the right wing was cut ($p < 3.13 \times 10^{-2}$, Tukey–Kramer *post hoc* comparison of the medians). Antennal motion on the side of the intact wing was the same as in control cases, except that the right antenna rotated slightly less caudally in response to the LT motion when the left wing was cut ($p < 9.48 \times 10^{-3}$, Tukey–Kramer *post hoc* comparison of the medians). During the baseline period before the onset of the visual motion, we observed that the antenna on the side of the intact wing rotated more caudally compared with the control cases ($p < 7.81 \times 10^{-3}$ and $p < 3.62 \times 10^{-2}$ for the left and right antenna, respectively, Tukey–Kramer *post hoc* comparison of the medians). This suggests that the induced flow field near each antenna is subtly influenced by the motion of the contralateral wing.

In contrast to the relatively small effect on the slow antennal motion, reducing the wing-induced flow had a large effect on the oscillation at WBF and its modulation during visually induced turns (Fig. 7*iii*,*iv*). Cutting the wing ipsilateral to an antenna significantly decreased oscillation of the antenna at WBF during the baseline period before the onset of visual motion compared with the control, or the cases in which the contralateral wing was cut ($p < 2.12 \times 10^{-3}$ and $p < 9.7 \times 10^{-3}$ for the left and right antenna, respectively, Tukey–Kramer *post hoc* comparison of the medians), providing additional evidence that wing-induced air currents are responsible for antennal oscillations at WBF. Furthermore, cutting the wing ipsilateral to an antenna reversed the way the antennal oscillations change during visually induced turns (Fig. 7*iii*,*iv*). When the left wing was intact, the fast oscillation of the left antenna increased during presentation of CW and RT stimuli and decreased during presentations of CCW and LT stimuli. However, when the left wing was cut, the fast oscillation of the left antenna decreased slightly during presentations of CW and RT stimuli and increased slightly during CCW and LT stimuli. The net result was significantly different compared with control flies ($p < 1.8 \times 10^{-7}$, $p < 9.02 \times 10^{-8}$, $p < 9.01 \times 10^{-7}$, and $p < 2.89 \times 10^{-5}$ for CW, RT, CCW, and LT motion, respectively, Wilcoxon's rank sum test for equal medians). The same reversal of the response occurred for the fast oscillations of the right antenna when the right wing was cut (response amplitudes significantly different from control flies, $p < 4.51 \times 10^{-8}$, $p < 2.03 \times 10^{-5}$, $p < 1.42 \times 10^{-8}$, and $p < 6.66 \times 10^{-8}$ for CW, RT, CCW, and LT motion, respectively, Wilcoxon's rank sum test for equal medians). These reversals of the responses may be attributable to an effect of the contralateral wing, which only becomes apparent when the contribution from the ipsilateral wing is reduced by the experimental manipulation.

Cutting the wing contralateral to an antenna did not significantly alter the oscillation of the antenna during the baseline period before the onset of the visual motion (Fig. 7*iii*,*iv*) ($p > 0.05$ for both the left and right antenna, Tukey–Kramer *post hoc* comparison of the medians). It also did not affect the magnitude of the increase in the oscillation during visually induced turns (Fig, 7*Aiii*,*Biii*,*Civ*,*Div*) ($p > 0.05$, Wilcoxon's rank sum test for equal medians). However, cutting the contralateral wing reduced the decrease in oscillation during visually induced turns (Fig. 7*Aiv*,*Biv*,*Ciii*,*Diii*). When the right wing was cut, the oscillation of the left antenna decreased significantly less in response to CCW and LT motion (Fig. 7*Ciii*,*Diii*) ($p < 5.98 \times 10^{-5}$ and $p < 2.76 \times 10^{-2}$ for CCW and LT motion, respectively, Wilcoxon's rank sum test for equal medians). When the left wing was cut, the oscillation of the right antenna decreased significantly less in response to CW motion (Fig. 7*Aiv*) ($p < 7.59 \times 10^{-4}$, Wilcoxon's rank sum test for equal medians) but not for RT motion (Fig. 7*Biv*) ($p > 0.05$, Wilcoxon's rank sum test for equal medians). These reductions of the decrease in oscillation that we observed when the contralateral wing was cut are probably attributable to the

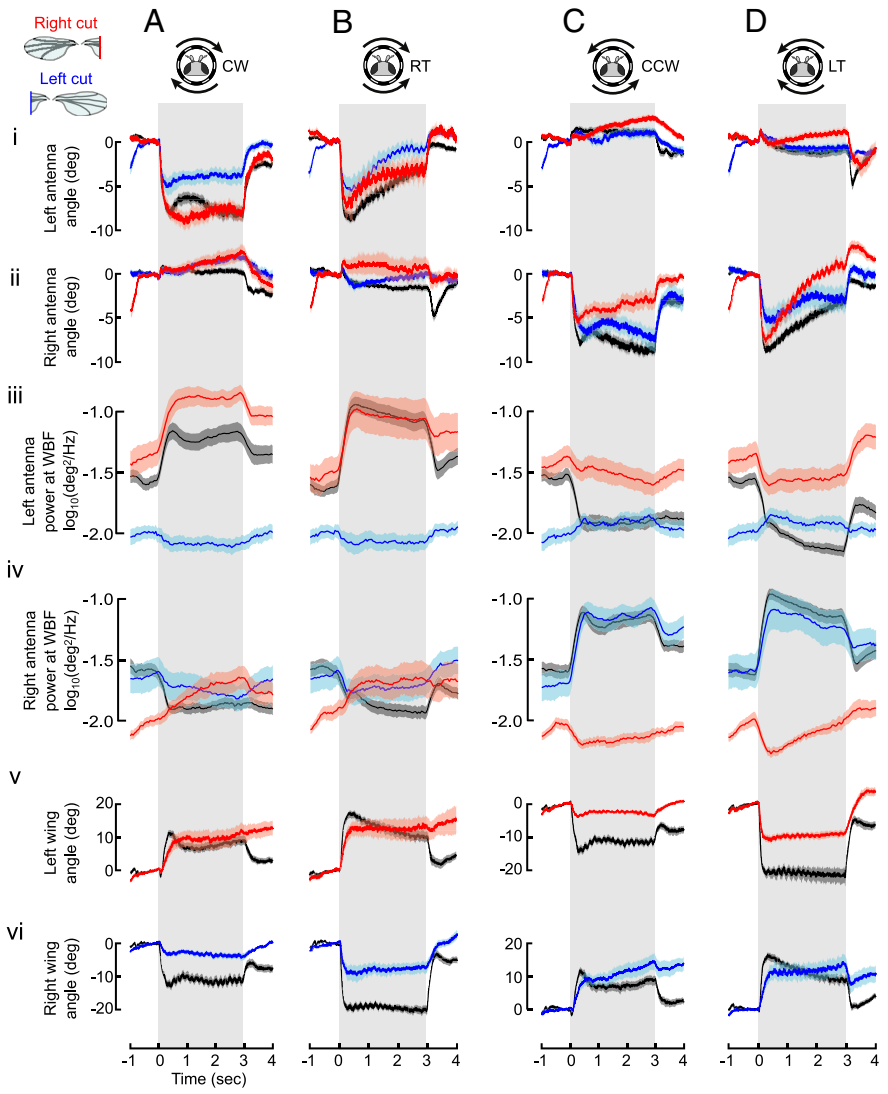

Figure 7. Reducing the wing induced air currents greatly alters the ipsilateral antennal oscillation at WBF and reduces the decrease in contralateral wing stroke amplitude but leaves the slow antennal motions relatively intact. ***A–D***, Mean ± SEM changes in the angles of the left (***i***) and right (***ii***) antenna, the mean ± SEM power of the oscillation at WBF (shown as $\log_{10}$ of the power) for the left (***iii***) and the right (***iv***) antenna, and the mean ± SEM changes in the angles of the left (***v***) and right (***vi***) wing during presentations of CW rotational (***A***), RT (***B***), CCW rotational (***C***), and LT (***D***) visual motion (areas shaded with light gray), in control (black), the right-wing-cut (red), and the left-wing-cut (blue) flies. Control data are from the same experiments as shown in Figure 2. For the right-wing-cut flies, sample sizes for CW rotational, RT, CCW rotational, and LT visual motions were 10, 7, 12, and 10, respectively. For the left-wing-cut flies, sample sizes were 10, 10, 8, and 8, respectively. Reducing the wing induced air currents by cutting the wing slightly decreased the slow caudal rotations of the ipsilateral antenna (***Ai***, ***Bi***, ***Cii***, ***Dii***) and greatly reduced the baseline oscillations of the ipsilateral antenna (***iii***, ***iv***). During presentations of visual motions, the magnitude of the antennal oscillation changed in a reverse direction to the control flies when ipsilateral wing was cut. Cutting the wing also reduced the decrease in the contralateral wing stroke amplitude during presentations of visual motions (***Avi***, ***Bvi***, ***Cv***, ***Dv***).

reduction of the decrease in ipsilateral wing stroke amplitude during visually induced turns in these flies as discussed below (Fig. 7*v*,*vi*).

Wing stroke amplitude decrease significantly less when contralateral wing is cut

Reducing the wing-induced airflow on one side created a situation in which passive antennal motion was greatly reduced while active antennal motion was left intact. This situation is the exact opposite of the SP joint gluing experiment and provided us with an opportunity to further investigate what type of antennal motion is responsible for activating the JO neurons that modify visually induced turning responses of the wing (Fig. 7*v*,*vi*). Results from the PF-joint-gluing experiments (Fig. 4) suggest that the main role of JO neurons in this behavior is to enhance the decrease in contralateral wing stroke amplitude. According to this hypothesis, cutting the wing on one side should affect wing stroke amplitude on the intact side during visually induced turns. Indeed, wing stroke amplitude decreased significantly less in response to rotational visual motion when the contralateral wing was cut (Fig. 7*Avi*,*Cv*) ($p < 5.66 \times 10^{-8}$ and $p < 8.567 \times 10^{-7}$ for the responses of left and right wings to CCW and CW motion, respectively, Wilcoxon's rank sum test for equal medians). Wing stroke amplitude also decreased less in response to translational visual motion when the contralateral wing was cut (Fig. 7*Bvi*,*Dv*) ($p < 1.39 \times 10^{-4}$ and $p < 9.25 \times 10^{-6}$ for the responses of the left and right wing to LT and RT motion, respectively, Wilcoxon's rank sum test for equal medians), although the percentage of the decrease was smaller than for the rotational visual motion. Consistent with the results from the PF-glued flies, cutting the contralateral wing did not significantly affect the increase in stroke amplitude at the onset of visual motion (Fig. 7*Av*,*Bv*,*Cvi*,*Dvi*) ($p > 0.05$, Wilcoxon's rank sum test for equal medians). Cutting the contralateral wing also significantly decreased wing stroke amplitude of the intact wing compared with controls during the baseline period before the onset of the visual motion ($p < 1.42 \times 10^{-2}$ and $p < 1.01 \times 10^{-2}$ for the left and right wing, respectively, Wilcoxon's rank sum test for equal medians) (data not shown). This low baseline when the contralateral wing was cut may have prevented wing stroke amplitude from decreasing as much as in controls in response to translational visual motion.

Discussion

Our results show that the antennae of *Drosophila* exhibit both large tonic rotations (Fig. 2) as well as small fast oscillations (Fig. 3) during visually induced turns. The tonic rotations are likely the combined result of a large active movement of the SP joint and a small passive deflection of the PF joint, whereas the fast oscillations represent passive motion of the PF joint (Figs. 4, 5). The active movements of the SP joint were absent in non-flying flies, suggesting that they play a role during flight, and are distinct from the visually mediated reflexes reported in other insects (Erber and Schildberger, 1980; Honegger, 1981; Ye et al., 2003). The passive movements of the PF joint increased when the angular distance between the antenna and wing stroke decreased and are most parsimoniously explained as a result of periodic wing-induced air currents (Figs. 3, 7). Active movements of the SP joint increased

the passive oscillations of the PF joint by bringing the wing and the antenna closer together (Fig. 5). Functionally, our experiments suggest that increases in the passive movements of the PF joint activate JO neurons that decrease stroke amplitude of the contralateral wing (Figs. 4–7). This feedback may enhance the turning responses by increasing the asymmetry of wing motion (Fig. 8).

Experiments in which we reduced activation of JO neurons provide evidence for a reflex pathway that regulates wing control muscles (Heide and Götz, 1996; Lehmann and Götz, 1996; Tu and Dickinson, 1996) (Fig. 4). During presentation of rotational visual motion, blocking JO function reduces the typical decrease in stroke amplitude of the contralateral wing and causes a delayed reduction of the increase in stroke amplitude of the ipsilateral wing (Fig. 4). These results suggest that activation of JO neurons normally decreases contralateral wing stroke amplitude and, more slowly, increases the ipsilateral wing stroke amplitude. Consistent with this hypothesis, inhibiting the JO of one antenna increases the baseline stroke amplitude of the contralateral wing and decreases the stroke amplitude of the ipsilateral wing (Fig. 4). Because increases in stroke amplitude activate JO neurons on the ipsilateral antenna and such activation decreases stroke amplitude of the contralateral wing, the reflex interaction results in mutual inhibition that could alone explain the positive influence of JO activation on ipsilateral stroke amplitude that we observed. Thus, the delayed increase in ipsilateral stroke amplitude may be attributable to the disinhibition of the reflex originating from the contralateral antenna.

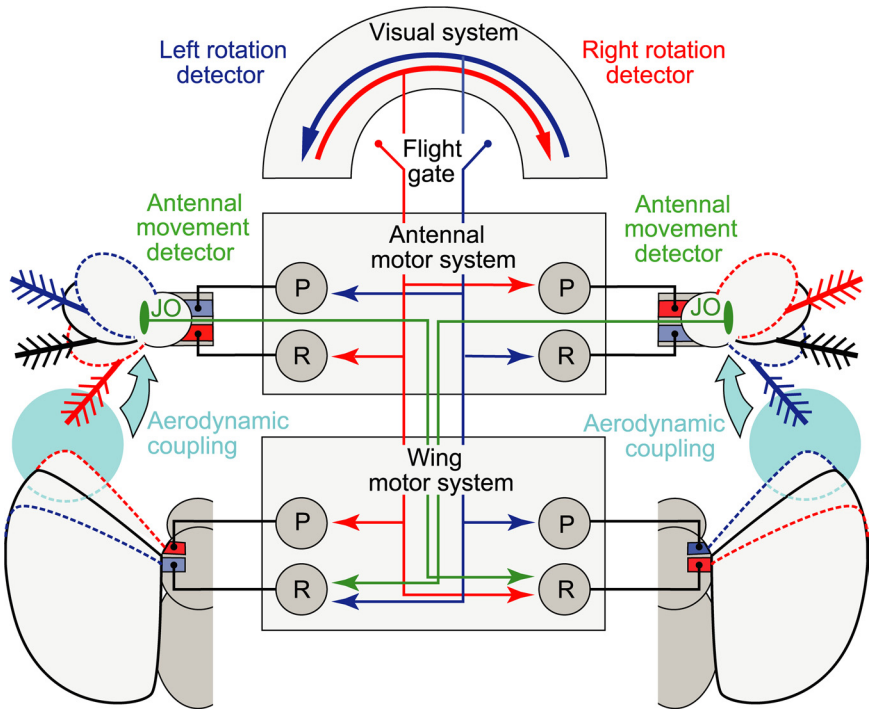

Figure 8. Schematic model for the optomotor responses of the antennae and its functional role during steering responses to rotational visual motions. Visual system detects rotational visual motion and activates both antennal and wing motor system to move the SP joint of the antennae in the direction opposite to that of the visual motion and the wing stroke envelope in the direction of the visual motion. Red and blue lines indicate visuomotor pathways activated by CW and CCW rotational visual motions, respectively. P and R indicate promotor and remoter and indicate activities of the motor systems that result in rostral and caudal movement of the antennae and the wings. Red and blue dotted lines show the positions of the antennae and the wings after the visuomotor response to CW and CCW rotational visual motions, respectively. This visuomotor response only happens during flight. The changes in the wing stroke envelope and the active movement of the SP joint bring the wing and the antenna closer on the side contralateral to the turn direction and increase the passive movements of the PF joint (i.e., both the small tonic deflection and the oscillation at WBF) by strengthening the aerodynamic coupling between the wing and the antenna. JO neurons detect the increase in the passive movements of the PF joint and activate wing motor system on the contralateral side to further reduce the wing stroke amplitude (green lines) and enhance the visually induced turn. This simple model would constitute a positive feedback system that would enhance differences in stroke amplitude in the initial stages of a visually mediated turn. Presumably, time dependencies within the system as well as feedback from other sensors, such as the halteres, would keep the system from pegging at one extreme.

Results from experiments in which we inhibited active antennal motion (Figs. 5, 6) and those in which we reduced wing-induced air currents (Fig. 7) suggest that either the increase in the oscillations of the PF joint or the tonic deflection of the PF joint could activate the reflex pathway to the wing motor system.

If antennal oscillations are critical, the magnitude of the oscillations that we observed (estimated to cause arista-tip displacements of ~2–15 μm) suggests that the JO neurons of the subgroups CDE, which can respond to oscillations of the arista-tip in the range of 0.1–4 μm (Kamikouchi et al., 2009), may be mediating the response. This is also consistent with the visually induced turning responses of the SP-glued flies, suggesting that the large antennal oscillations may be saturating the responses of the mechanosensory neurons involved (Figs. 5, 6). The JO neurons of the subgroups CE are preferentially activated by large static deflections of the arista tip (5 μm to 100 μm) (Kamikouchi et al., 2009; Yorozu et al., 2009) and may also encode the tonic deflection of the PF joint that we observed (estimated to be ~1–7 μm). However, without direct recordings from these neurons during flight, it is difficult to determine exactly which neurons are mediating these reflexes.

The hypothesis that the activation of JO neurons decreases the contralateral wing stroke amplitude is not well supported by our experiments using translational visual motion (Fig. 4). One possible explanation for this discrepancy is that the stronger turning responses induced by translational motion mask the influence of JO neurons on wing muscles. However, in preliminary experiments using translational motion with slower temporal frequency, blocking the JO function did not result in expected changes in stroke amplitude even when the turning responses induced by translational motion were weaker (data not shown). Another possibility is that, because distinct premotor circuits are thought to mediate the responses to the rotational and translational motion (Duistermars et al., 2007), the influence of the JO afferents on these responses is also different. Previous studies using magnetically tethered flies, which can rotate freely around their yaw axis, have also yielded different effects of JO interference on different types of orientation responses (Budick et al., 2007; Duistermars et al., 2009).

We performed all experiments in head-fixed flies because head movements can interfere with our measurements of antennae motion. Preliminary observations show that tethered flies move their head in the direction of the visual motion when their heads are not restrained (data not shown). This head movement

is likely to position the antenna on the outside of the turn farther away from the induced flow field of the wings and reduce the passive movements of the PF joint. However, head movements were small compared with the movements of wing stroke envelope during visually induced turns, suggesting that passive antennal movements will still increase during turns even in head-free flies. Furthermore, although it has been shown that freely flying blowflies move their head during turns to stabilize gaze (Schilstra and van Hateren, 1998), we have not been able to confirm head movements in freely flying *Drosophila* (our unpublished data), suggesting that the head movements observed in *Drosophila* may be in part an artifact of tethered conditions. Although direct evidence from free flight is lacking and will be difficult to collect because of the spatial resolution required, we believe that the passive antennal movements and consequent enhancement of the visually induced turns we observed in head-fixed tethered flies is also likely to take place in freely flying *Drosophila*.

Although blocking the active movements of the SP joint did not significantly affect the visually induced turns in our head-fixed, tethered flies, the strong correlation with ipsilateral wing stroke amplitude (Figs. 2, 4) suggests that it may play some role during turns in free flight. If freely flying *Drosophila* do move their head during turns, active antennal movements will work to keep the antennae at the same relative angle to the body by rotating the antenna in the direction opposite to the head motion. Because evidence suggests that *Drosophila* use their antennae to detect the orientation of the wind (Budick et al., 2007), this compensation may allow the flies to keep track of the wind direction relative to the body orientation during the turn despite the yaw rotation of the head. If freely flying *Drosophila* do not move their head during turns, the role of active antennal movements may be to keep the antennae at the same relative angle against the airflow generated by self-motion. Because of the inertia of the body at the very start of a turn (Dickson et al., 2010), the longitudinal axis of the fly's body may not be tangent to the flight path. Such a mismatch might evoke an antenna-mediated upwind orientation response (Budick et al., 2007) that would act to oppose the turn. Active rotation of the antennae toward the direction opposite to that of the turn might function to alleviate this potential conflict by maintaining the antenna at the same relative angle to the airflow even when the orientation of the fly's body is not tangent to the flight path. Finally, active movement of the antenna might function to enhance visually induced turns in some situations by bringing the antenna and the wing closer together to further increase passive movements of the PF joint. We did find that active antennal motion significantly enhanced the magnitude of antennal oscillation during turns (Fig. 5), but this enhancement did not significantly affect the turning responses in our tethered flies (Fig. 6). One explanation for this lack of effect is that, in response to strong visual stimuli, the increase in ipsilateral wing stroke amplitude alone is sufficient to increase antennal oscillation and saturate the JO neurons. However, this saturation might not occur in free flight because three-dimensional high-speed video analysis indicates that the changes in wing stroke amplitude during free flight turns (Fry et al., 2003) are much less than what we observed in tethered flies.

High-resolution analysis of antennal movements and wing motions during free flight together with genetic (White et al., 2001) and optogenetic (Miesenböck and Kevrekidis, 2005) manipulations to alter the activity of specific groups of JO neurons should further clarify the functional roles of each type of antennal movements we have described in this paper. Understanding how flies move their antennae and how they use mechanosensory information during visually induced turns will provide us with additional insights into how animals obtain and integrate sensory information from multiple modalities to produce context-appropriate motor patterns.

References

Baba Y, Comer CM (2008) Antennal motor system of the cockroach, *Periplaneta americana.* Cell Tissue Res 331:751–762.

Bauer CK, Gewecke M (1991) Motoneuronal control of antennal muscles in *Locusta migratoria.* J Insect Physiol 37:551–562.

Budick SA, Dickinson MH (2006) Free-flight responses of *Drosophila melanogaster* to attractive odors. J Exp Biol 209:3001–3017.

Budick SA, Reiser MB, Dickinson MH (2007) The role of visual and mechanosensory cues in structuring forward flight in *Drosophila melanogaster*. J Exp Biol 210:4092–4103.

Burkhardt D, Gewecke M (1965) Mechanoreception in Arthropoda: the chain from stimulus to behavioral pattern. Cold Spring Harb Symp Quant Biol 30:601–614.

Caldwell JC, Eberl DF (2002) Towards a molecular understanding of *Drosophila* hearing. J Neurobiol 53:172–189.

Cullen KE (2004) Sensory signals during active versus passive movement. Curr Opin Neurobiol 14:698–706.

Dickinson MH, Götz KG (1996) The wake dynamics and flight forces of the fruit fly *Drosophila melanogaster*. J Exp Biol 199:2085–2104.

Dickson WB, Polidoro P, Tanner MM, Dickinson MH (2010) A linear systems analysis of the yaw dynamics of a dynamically scaled insect model. J Exp Biol 213:3047–3061.

Duistermars BJ, Frye MA (2010) Multisensory integration for odor tracking by flying *Drosophila*: behavior, circuits and speculation. Commun Integr Biol 3:60–63.

Duistermars BJ, Chow DM, Condro M, Frye MA (2007) The spatial, temporal and contrast properties of expansion and rotation flight optomotor responses in *Drosophila.* J Exp Biol 210:3218–3227.

Duistermars BJ, Chow DM, Frye MA (2009) Flies require bilateral sensory input to track odor gradients in flight. Curr Biol 19:1301–1307.

Dürr V, König Y, Kittmann R (2001) The antennal motor system of the stick insect *Carausius morosus*: anatomy and antennal movement pattern during walking. J Comp Physiol A 187:131–144.

Eberl DF, Hardy RW, Kernan MJ (2000) Genetically similar transduction mechanisms for touch and hearing in *Drosophila.* J Neurosci 20:5981–5988.

Egelhaaf M, Borst A (1989) Transient and steady-state response properties of movement detectors. J Opt Soc Am A 6:116–127.

Ehmer B, Gronenberg W (1997) Antennal muscles and fast antennal movements in ants. J Comp Physiol B Biochem Syst Environ Physiol 167:287–296.

Erber J, Schildberger K (1980) Conditioning of an antennal reflex to visual-stimui in bees (*Apis mellifera L*). J Comp Physiol 135:217–225.

Ewing AW (1978) Antenna of *Drosophila* as a love song receptor. Physiol Entomol 3:33–36.

Fry SN, Sayaman R, Dickinson MH (2003) The aerodynamics of free-flight maneuvers in *Drosophila*. Science 300:495–498.

Gewecke M (1970) Antennae: another wind sensitive receptor in locusts. Nature 225:1263–1264.

Gewecke M, Schlegel P (1970) Die Schwingungen der Antenne und ihre Bedeutung für die Flugsteuerung bei *Calliphora erythrocephala.* Z Vergleich Physiol 67:325–362.

Göpfert MC, Robert D (2001) Biomechanics: turning the key on *Drosophila* audition. Nature 411:908.

Göpfert MC, Robert D (2002) The mechanical basis of *Drosophila* audition. J Exp Biol 205:1199–1208.

Götz KG (1964) Optomotorische untersuchung des visuellen systems einiger augenmutanten der fruchtfliege *Drosophila.* Kybernetik 2:77–92.

Götz KG (1987) Course-control, metabolism and wing interference during ultralong tethered flight in *Drosophila melanogaster*. J Exp Biol 128:35–46.

Götz KG, Hengstenberg B, Biesinger R (1979) Optomotor control of wing beat and body posture in *Drosophila.* Biol Cybern 35:101–112.

Hartenstein V (2006) The muscle pattern of *Drosophila.* In: Muscle development in *Drosophila* (Sink H, ed), pp 8–27. Austin, TX: Landes Bioscience/Eurekah.com; Springer Science+Business Media.

Heide G, Götz KG (1996) Optomotor control of course and altitude in *Dro-*

sophila melanogaster is correlated with distinct activities of at least three pairs of flight steering muscles. J Exp Biol 199:1711–1726.

Heisenberg M, Wolf R (1984) Vision in *Drosophila*: genetics of microbehavior. Berlin: Springer.

Heran H (1959) Wahrnehmung und regelung der flugeigengeschwindigkeit bei *Apis-mellifica L.* Z Vergleich Physiol 42:103–163.

Hesselberg T, Lehmann FO (2009) The role of experience in flight behaviour of *Drosophila.* J Exp Biol 212:3377–3386.

Honegger HW (1981) A preliminary note on a new optomotor response in crickets: antennal tracking of moving targets. J Comp Physiol 142:419–421.

Honegger HW, Allgäuer C, Klepsch U, Welker J (1990) Morphology of antennal motoneurons in the brains of 2 crickets, *Gryllus bimaculatus* and *Gryllus campestris*. J Comp Neurol 291:256–268.

Johnston C (1855) Auditory apparatus of the *Culex* mosquito. Q J Microsc Sci 3:97–102.

Kamikouchi A, Inagaki HK, Effertz T, Hendrich O, Fiala A, Göpfert MC, Ito K (2009) The neural basis of *Drosophila* gravity-sensing and hearing. Nature 458:165–171.

Kloppenburg P (1995) Anatomy of the antennal motoneurons in the brain of the honeybee (*Apis mellifera*). J Comp Neurol 363:333–343.

Kloppenburg P, Camazine SM, Sun XJ, Randolph P, Hildebrand JG (1997) Organization of the antennal motor system in the sphinx moth *Manduca sexta.* Cell Tissue Res 287:425–433.

Lehmann FO, Dickinson MH (1997) The changes in power requirements and muscle efficiency during elevated force production in the fruit fly *Drosophila melanogaster.* J Exp Biol 200:1133–1143.

Lehmann FO, Götz KG (1996) Activation phase ensures kinematic efficacy in flight-steering muscles of *Drosophila melanogaster*. J Comp Physiol A 179:311–322.

Maddess T (1986) Afterimage-like effects in the motion-sensitive neuron H1. Proc R Soc Lond B Biol Sci 228:433–459.

Maimon G, Straw AD, Dickinson MH (2010) Active flight increases the gain of visual motion processing in *Drosophila.* Nat Neurosci 13:393–399.

Miesenböck G, Kevrekidis IG (2005) Optical imaging and control of genetically designated neurons in functioning circuits. Annu Rev Neurosci 28:533–563.

Mitra P, Bokil H (2008) Observed brain dynamics. New York: Oxford UP.

Poelma C, Dickson WB, Dickinson MH (2006) Time-resolved reconstruction of the full velocity field around a dynamically-scaled flapping wing. Exp Fluids 41:213–225.

Reichardt W, Wenking H (1969) Optical detection and fixation of objects by fixed flying flies. Naturwissenschaften 56:424–425.

Reiser MB, Dickinson MH (2008) A modular display system for insect behavioral neuroscience. J Neurosci Methods 167:127–139.

Robie AA, Straw AD, Dickinson MH (2010) Object preference by walking fruit flies, *Drosophila melanogaster*, is mediated by vision and graviperception. J Exp Biol 213:2494–2506.

Sane SP, Dieudonné A, Willis MA, Daniel TL (2007) Antennal mechanosensors mediate flight control in moths. Science 315:863–866.

Schilstra C, van Hateren JH (1998) Stabilizing gaze in flying blowflies. Nature 395:654.

Schneider D (1964) Insect antennae. Annu Rev Entomol 9:103–122.

Schroeder CE, Wilson DA, Radman T, Scharfman H, Lakatos P (2010) Dynamics of active sensing and perceptual selection. Curr Opin Neurobiol 20:172–176.

Straw AD, Dickinson MH (2009) Motmot, an open-source toolkit for realtime video acquisition and analysis. Source Code Biol Med 4:5.

Tammero LF, Frye MA, Dickinson MH (2004) Spatial organization of visuomotor reflexes in *Drosophila.* J Exp Biol 207:113–122.

Tu MS, Dickinson MH (1996) The control of wing kinematics by two steering muscles of the blowfly (*Calliphora vicina*). J Comp Physiol A 178:813–830.

White B, Osterwalder T, Keshishian H (2001) Molecular genetic approaches to the targeted suppression of neuronal activity. Curr Biol 11:R1041–R1053.

Ye S, Leung V, Khan A, Baba Y, Comer CM (2003) The antennal system and cockroach evasive behavior. I. Roles for visual and mechanosensory cues in the response. J Comp Physiol A Neuroethol Sens Neural Behav Physiol 189:89–96.

Yorozu S, Wong A, Fischer BJ, Dankert H, Kernan MJ, Kamikouchi A, Ito K, Anderson DJ (2009) Distinct sensory representations of wind and near-field sound in the *Drosophila* brain. Nature 458:201–205.